Image-based assessment of plant disease progression identifies new genetic loci for resistance

Valérian Méline[a], Denise L. Caldwell[a], Bong-Suk Kim[a], Sriram Baireddy[b], Changye Yang[b], Erin E. Sparks[c], Edward J. Delp[b], and Anjali S. Iyer-Pascuzzi[a†]

[a] 915 W. State Street, Department of Botany and Plant Pathology, Purdue University, West Lafayette, Indiana, USA
[b] Video and Image Processing Laboratory (VIPER), School of Electrical and Computer Engineering
[c] Department of Plant and Soil Sciences and the Delaware Biotechnology Institute, University of Delaware, Newark, DE

†Author for correspondence: asi2@purdue.edu

Keywords: Digital phenotyping, QTL, *Ralstonia*, bacterial wilt, tomato

Running title: Disease resistance QTL from image-based phenotyping

Abstract

A major challenge in global crop production is mitigating yield loss due to plant diseases. One of the best means of disease control is plant resistance, but the identification of genes that promote resistance has been limited by the subjective quantification of disease, which is typically scored by the human eye. We hypothesized that image-based quantification of disease phenotypes would enable the identification of new disease resistance loci. We tested this using the interaction between tomato and *Ralstonia solanacearum*, a soilborne pathogen that causes bacterial wilt disease. We acquired over 40,000 time-series images of disease progression in a tomato recombinant inbred line population, and developed an image analysis pipeline providing a suite of ten traits to quantify wilt disease based on plant shape and size. Quantitative trait loci (QTL) analyses using image-based phenotyping identified QTL that were both unique and shared compared with those identified by human assessment of wilting. When shared loci were identified, image-based phenotyping could detect some QTL several days earlier than human assessment. Thus, expanding the phenotypic space of disease with image-based phenotyping allowed both earlier detection and identified new genetic components of resistance.

18 **Main**

19 Plant diseases are a significant global constraint to crop production. Developing disease resistant
20 crops requires identifying the plant genomic regions and genes that contribute to resistance to the
21 pathogenic microbes that cause disease. This in turn depends on phenotyping large populations
22 of plants for their responses to pathogens. Phenotyping plant diseases is challenging because
23 diseases cause complex, quantitative phenotypes that can occur at different scales – e.g. on parts
24 of leaves, entire leaves, or the whole plant. In addition, disease phenotypes vary over time and
25 depend on environmental conditions, plant age, and pathogen virulence. Disease symptoms such
26 as wilting or necrotic spots have traditionally been scored with the human eye, but these scores
27 are subjective, can vary by individual, and are difficulty to accurately quantify.

28

29 The challenging nature of visual disease assessment has led to the use of sensors including RGB,
30 hyperspectral, chlorophyll fluorescence and thermal cameras to assess disease symptoms [1–7].
31 Compared to assessment by the human eye, image-based phenotyping is faster, more
32 reproducible, and more sensitive to small variations in disease symptoms that can be critical for
33 detecting resistance loci [3–5,8–10]. Although many studies have used or developed tools to assess
34 plant symptoms using different types of sensors [4–7,11–16], few studies have used these
35 technologies in QTL or Genome Wide Association (GWA) analyses for responses to plant
36 pathogens.

37

38 The soil-borne betaproteobacterium *Ralstonia solanacearum* is the causal agent of bacterial wilt
39 disease and has been ranked as one of the top 10 most destructive plant bacterial pathogens of all
40 time [17]. *Ralstonia* infection causes susceptible plants to wilt, and the amount of wilting correlates

41 with a plant's level of susceptibility [18,19]. The bacterium is a major production constraint in
42 Solanaceous crops both globally and in the United States, where disease loss in tomatoes can
43 exceed 70%. In crops, resistance to *Ralstonia* is quantitative, but the quantitative trait loci (QTL)
44 underlying resistance to US strains of *Ralstonia* are largely unknown. QTL for other strains have
45 been mapped [20–27] but have not been cloned, and the host determinants necessary for resistance
46 remain mostly unspecified.
47
48 The limited identification of QTL for *Ralstonia* resistance can be attributed in part to the
49 difficulty in accurately scoring plant wilting. Wilting is traditionally measured on a 0 – 4 scale,
50 in which 0 indicates a plant with no wilting, 1 = 1 – 25%, 2 = 26 – 50%, 3 = 51 – 75% and a
51 score of 4 indicates a plant with 76 – 100% wilted leaves [28]. While it is straightforward to assess
52 the ends of the spectrum, rating plants with scores of 2 or 3 is particularly difficult. This is due to
53 the subjective nature of visually determining when a leaf has lost sufficient turgor to qualify as
54 wilted. Reliable disease phenotyping is critical for identifying QTL for resistance to *Ralstonia*
55 and the development of resistant varieties.
56
57 Here, we used image-based phenotyping to identify new tomato genetic resistance loci to
58 *Ralstonia*. We developed a semi-automated imaging and trait analysis pipeline to quantify
59 bacterial wilt disease in a recombinant inbred line (RIL) population derived from *Ralstonia*-
60 resistant and susceptible tomato genotypes. We found both unique and shared QTL between our
61 image-based traits and plant wilting scored by the human eye. At least one of the QTL was
62 detected by image-based phenotyping before the onset of visual symptoms, demonstrating that
63 image-based phenotyping captures the disease phenotype at early stages of infection. These

64 results demonstrate that imaged-based phenotyping can shed light on new aspects of disease and
65 improve our ability to identify genetic loci crop resistance.

66 **Results**

67 *Development of an aboveground imaging and semi-automated analysis pipeline*

68 We first constructed a simple, low-cost imaging system that allowed us to semi-automate
69 aboveground disease phenotyping. Each plant was placed on a commercially available turntable,
70 and plants were imaged with a Canon DSLR (Supplementary Figure 1; details in methods). The
71 turntable and camera were connected with Photocapture 360 (Ortery technologies), which
72 allowed us to automatically capture images every 45 degrees (8 images per plant). Each image
73 included a fiducial marker for post-image color correction. Plants in the F_9 generation from a
74 RIL population derived from a cross between resistant Hawaii 7996 (H7996) and susceptible
75 West Virginia 700 (WV) were imaged the day before inoculation with *R. solanacearum* strain
76 K60, and at 3, 4, 5 and 6 days post inoculation (dpi). At 3 dpi, symptoms were not present in
77 susceptible parent WV, but by 6 dpi these plants were completely wilted. We imaged five
78 replicate plants of each RIL as well as the parental lines. Using this system, we captured over
79 40,000 images for high-resolution disease phenotyping. The same set of plants was also visually
80 scored by the human eye at 8 dpi. Visual scoring was based on the percentage of wilted leaves.
81 Tomato phenotypes in the RIL population ranged from highly susceptible to highly resistant,
82 consistent with the quantitative nature of disease resistance (Supplementary Figures 2 and 3).
83

84 We next developed a set of mathematical descriptors to phenotype wilting over time in our
85 images. We used 10 image-based traits (Table 1) to describe different aspects of plant wilting:
86

87

		Hawaii 7996				West Virginia 700				RILs			
year	Variable	Mean	SD	Minimum	Maximum	Mean	SD	Minimum	Maximum	Mean	SD	Minimum	Maximum
2016	Wilting_Score	0	0	0	0	100	0	100	100	44.41	41.4	0	100
	Wilting_Score	0	0	0	0	99.33	5.16	60	100	53.69	42.23	0	100
	convex area	2.7e+06	1.4e+06	-4.1e+04	6.3e+06	-3.6e+05	3.6e+05	-1.1e+06	7.4e+05	1.2e+06	1.4e+06	-2.0e+06	7.9e+06
	convex width	8.7e+02	4.4e+02	-7.0e+01	1.7e+03	-7.4e+02	3.7e+02	-1.4e+03	5.4e+02	-4.6e-01	5.9e+02	-1.9e+03	2.9e+03
	plant area	8.7e+05	5.6e+05	-1.0e+04	2.2e+06	-1.1e+05	1.1e+05	-3.4e+05	2.1e+05	5.0e+05	5.5e+05	-7.4e+05	2.6e+06
	plant height	5.6e+02	1.9e+02	-7.0e+01	8.7e+02	-1.3e+01	1.7e+02	-3.6e+02	3.7e+02	3.3e+02	2.5e+02	-6.5e+02	1.1e+03
2019	plant width	4.0e+02	2.0e+02	-3.6e+01	8.2e+02	-3.5e+02	1.8e+02	-6.6e+02	2.5e+02	-2.1e+01	2.7e+02	-9.7e+02	8.4e+02
	X mass	3.1e+02	1.6e+02	-3.7e+01	5.8e+02	-2.9e+02	1.5e+02	-5.6e+02	2.0e+02	-1.2e+01	2.3e+02	-7.4e+02	6.9e+02
	Y mass	5.4e+02	2.1e+02	-8.4e+01	9.3e+02	-6.7e+01	1.6e+02	-4.1e+02	3.6e+02	2.1e+02	2.2e+02	-7.0e+02	9.6e+02
	CM width	3.1e+02	1.6e+02	-1.0e+02	6.0e+02	-2.9e+02	1.5e+02	-5.2e+02	1.8e+02	2.7e+01	2.3e+02	-7.0e+02	9.8e+02
	CM height	2.6e+02	1.8e+02	-2.1e+02	6.2e+02	-1.3e+02	1.5e+02	-3.9e+02	1.9e+02	-5.2e+01	1.9e+02	-8.8e+02	8.3e+02
	color average	2.88	5.44	-5.96	22.9	7.37	2.84	1.03	14.83	4.06	4.48	-11.35	16.48

Table 1 Descriptive statistics for 10 image-based traits and two years of visually assessed wilting scores (2016 and 2019). Image-based traits were from the same plants as the visually assessed wilting score in 2019. The RIL population was inoculated with Ralstonia and visually scored for wilting in 2016, but images were not taken. Data is shown for resistant parent Hawaii 7996, susceptible parent West Virginia 700, and the RIL population.

88 convex area, convex width, plant area, plant height, plant width, X mass, Y mass, center of mass
89 (CM) height, CM width, and color. Several of these, such as the area and width of the convex
90 hull, are traditional methods of describing aboveground plant shape. Because the center of mass
91 of a plant leaf changes as a plant wilts, we developed additional descriptors based on the distance
92 of the leaf center of mass from the stem (CM width and CM height, X mass and Y mass). We
93 then developed a pipeline which used the original image as input, performed color correction,
94 and quantified each descriptor (Figure 1 and Supplementary Figure 4, and methods).

95

96 *Image-based traits differentiate resistant and susceptible plants*

97 To validate the efficiency of the image-based descriptors to estimate wilting phenotypes, we
98 tested whether image-based phenotyping descriptors could differentiate resistant from
99 susceptible plants. Supplementary Figure 5 shows the average normalized score for each of the
100

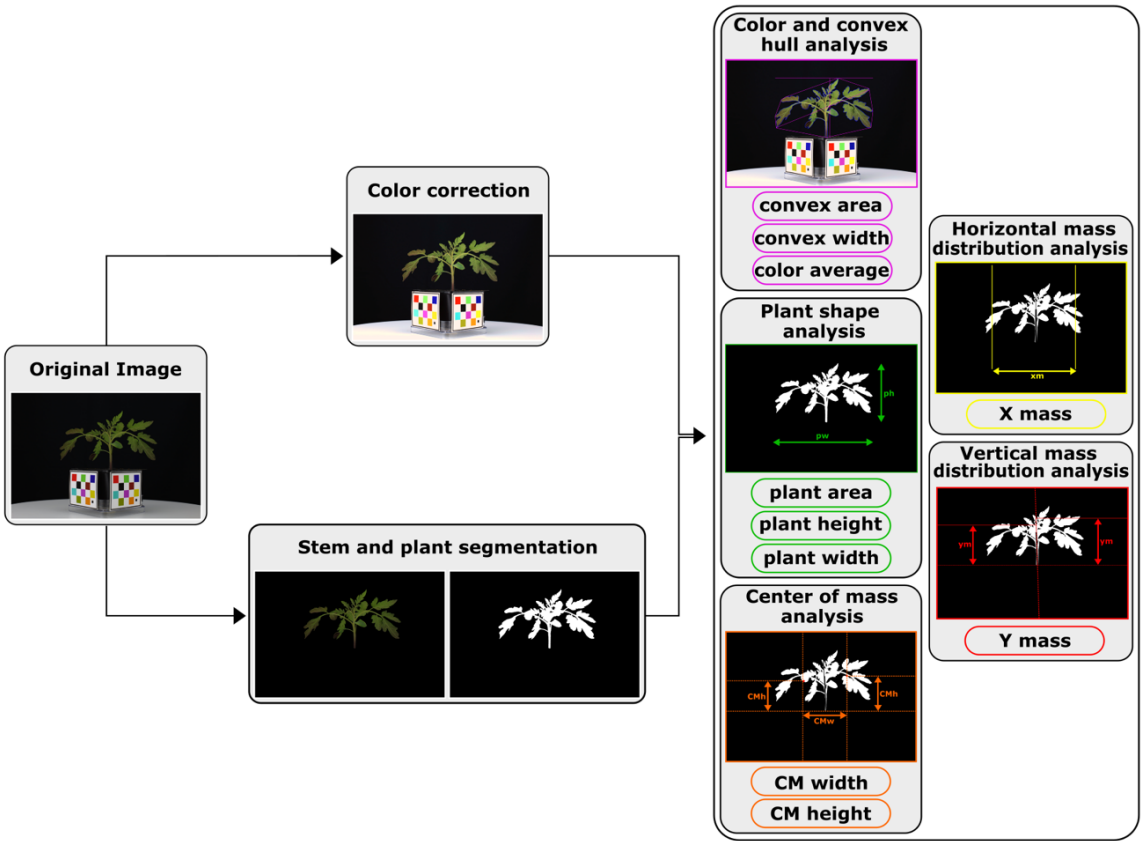

Figure 1: Diagram of the semi-automated analysis pipeline and 10 image descriptors

image-based descriptors for each parent and the RIL population from -1 (the day before inoculation) to 6 dpi. Most descriptors, particularly those based on plant width or convex hull, had clearly divergent values in resistant and susceptible plants at a given time point. RIL descriptor values ranged from those of the resistant to susceptible parents and occasionally showed transgressive segregation (Supplementary Figure 5). Because plant shape at 6 dpi depends on shape of the same plant at -1 dpi, we used the evolution of each descriptor from day -1 to 6 dpi in our QTL analysis. This evolution was termed a ‘trait’. Trait values were clearly different for resistant and susceptible parents for all traits except color (Figure 2), which was not used further.

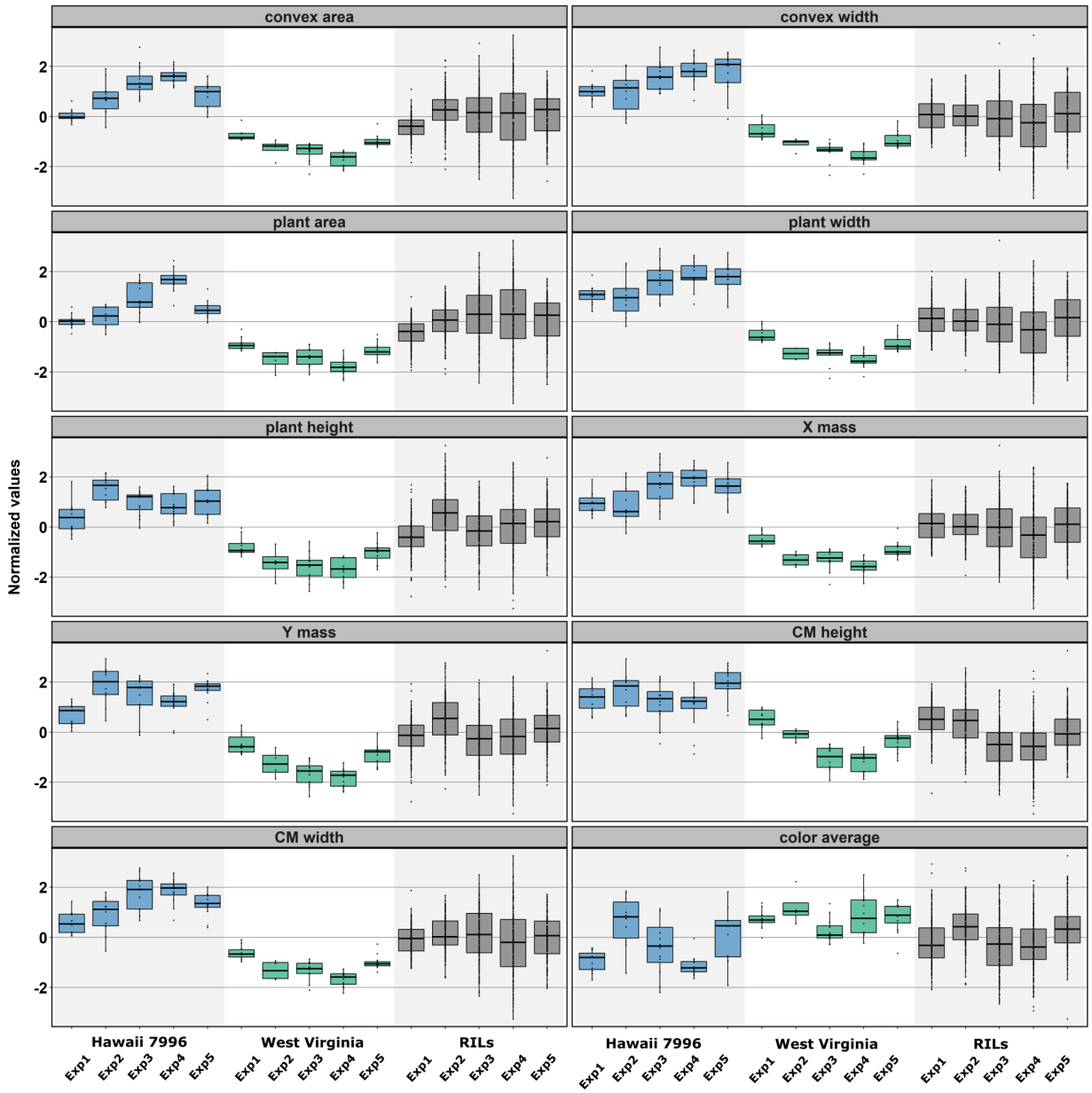

Figure 2: Boxplots showing the evolution of the normalized values between -1 and 6 dpi for each of the five biological replicates for the 10 image-based traits for resistant Hawaii 7996, susceptible West Virginia parents and the 166 RILs. Color was unable to differentiate resistant from susceptible plants and was not used further.

Image-based phenotyping reveals drivers of the wilting phenotype

We next investigated whether any of our traits were major components of the wilting phenotype.

We visually scored plants and asked how well our image-based traits correlated with human

visual scoring. Wilting is categorized by loss of plant leaf turgor that results in drooping leaves, and decreased plant width and height. Determining how much a plant has wilted is challenging, in part because it can be difficult to quantify how much each a leaf has drooped and how much drooping of one leaf correlates with whole plant wilting.

We aimed to quantify leaf drooping using center of mass traits. Among our image-based traits, those which were functions of the leaf center of mass were highly inversely correlated with visual wilting (i.e. as a plant wilts, the center of mass decreases), suggesting that these are major drivers of the wilting phenotype. These traits included CM width, plant width and X mass (r > -0.75) (Figure 3).

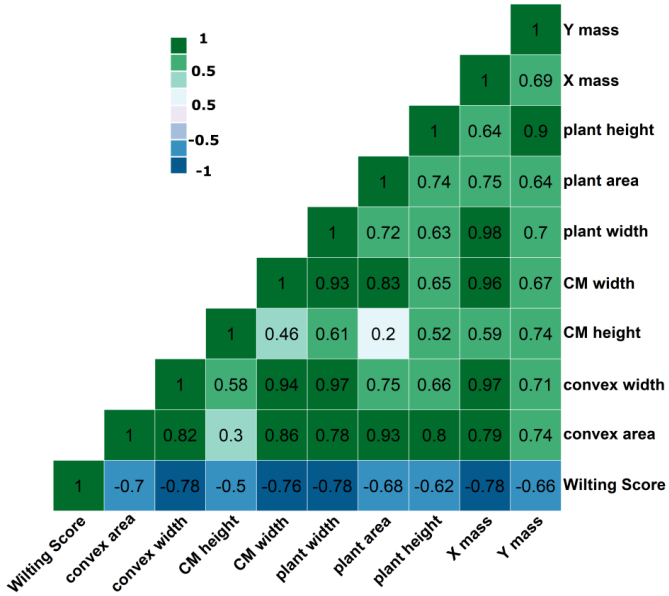

Figure 3: Heatmap showing the Pearson correlation values between image-based traits used in our QTL analysis and the human eye based wilting score in 2019. The correlations values were determined using the same plants imaged and visually assessed in 2019.

Several of our traits describe similar aspects of plant shape, such as height or width, through different methods. These traits tended to be highly correlated with each other. For example, plant height vs Y mass use different methods to describe plant width (based on the plant mask or the

135 center of mass of the stem masks; see Methods), and were highly positively correlated with each
136 other (0.93; Figure 3).
137
138 We trained a random forest, consisting of 1000 decision trees, to use data from 6 dpi to predict
139 the expert visual score assigned at 8 dpi. We used 969 plants in a 60:40 training-testing data
140 split, and achieved a classification accuracy of 83%. To identify the traits that provided the most
141 efficient estimation of wilting symptoms, we randomly scrambled the nine image-based traits
142 one at a time. Plant width and plant area had the most impact on wilting score prediction
143 (Supplementary Figure 6).
144
145 *QTL analysis identifies 20 wilting QTL in 10 clusters across the tomato genome at 6 dpi*
146 Our overall goal was to identify tomato genomic regions that provide resistance or susceptibility
147 to *Ralstonia*. Prior to this analysis, we first generated a genetic map using Genotyping-by-
148 Sequencing (GBS). We identified 632 high-quality SNPs for linkage mapping using GBS. We
149 combined these with 112 SolCap markers, and subsequently generated a linkage map using ICI
150 mapping software [29]. Our linkage map consisted of ~1300 cM (Figure 4) with an average per
151 chromosome marker density that varies from 1.8 to 7.48 cM (Supplementary Table 1).
152
153 For QTL analysis, we mapped the evolution of each our nine image-based descriptors from -1 to
154 6 dpi. In addition to the image-based phenotyping, we used two years (2016 and 2019) of
155 visually scored phenotyping data at 8 dpi. Visually assessed wilt scores from 2019 were
156 quantified from the same plants that were used for image-based phenotyping. In 2016, plants
157 were only visually scored for wilting, and no image-based measurements were taken. Using ICI

158 mapping software and composite interval mapping (CIM) for all traits, we identified 20 QTL
159 within the RIL population with a LOD score above 3 (Table 2). To be consistent with previous
160 studies of tomato-*Ralstonia* QTL mapping, we call these QTL, 'Bacterial wilt resistance (*Bwr*)
161 QTL'. Each *Bwr* QTL explained approximately 6 to 11% of the variation in response to *R.*
162 *solanacearum* strain K60.
163

Chromosome	Cluster	Position	LeftMarker	RightMarker	TraitName	LOD	PVE	Add	LeftCI	RightCI
2	Bwr2.1	45	solcap_snp_sl_18519	SL3.0ch02-49265134	plant width	3.4108	6.4576	-0.1669	42.5	47.5
2	Bwr2.2	72	SL3.0ch02-45885016	SL3.0ch02-44375028	X mass	3.4765	9.4924	-0.2178	69.5	73.5
2	Bwr2.2	72	SL3.0ch02-45885016	SL3.0ch02-44375028	CM width	3.2455	8.455	-0.2189	69.5	73.5
3	Bwr3.1	22	solcap_snp_sl_14355	solcap_snp_sl_9689	convex width	5.3238	10.2506	0.2103	21.5	26.5
3	Bwr3.1	22	solcap_snp_sl_14355	solcap_snp_sl_9689	plant width	4.7309	9.1511	0.1976	21.5	25.5
3	Bwr3.1	22	solcap_snp_sl_14355	solcap_snp_sl_9689	X mass	3.4765	5.8012	0.1705	21.5	26.5
3	Bwr3.1	23	solcap_snp_sl_14355	solcap_snp_sl_9689	CM width	3.6627	6.2716	0.1887	21.5	27.5
3	Bwr3.1	25	solcap_snp_sl_14355	solcap_snp_sl_9689	plant height	4.5107	7.6902	0.1896	21.5	31.5
3	Bwr3.1	25	solcap_snp_sl_14355	solcap_snp_sl_9689	Y mass	3.3918	9.3283	0.1708	21.5	31.5
3	Bwr3.2	38	solcap_snp_sl_21215	solcap_snp_sl_9663	Wilting Score 2016	3.5258	7.3736	-0.1726	35.5	39.5
3	Bwr3.2	38	solcap_snp_sl_21215	solcap_snp_sl_9663	convex area	3.4328	9.0796	0.1953	34.5	39.5
3	Bwr3.2	38	solcap_snp_sl_21215	solcap_snp_sl_9663	plant area	3.3019	8.6697	0.1902	34.5	39.5
4	Bwr4.1	4	SL3.0ch04-60431371	solcap_snp_sl_11543	convex width	3.1855	6.0199	0.1627	1.5	10.5
5	Bwr5.1	100	solcap_snp_sl_22649	SL3.0ch05-65105663	plant height	3.6115	9.4852	0.2103	95.5	103.5
6	Bwr6.1	79	solcap_snp_sl_14458	SL3.0ch06-39435402	Wilting Score 2016	4.077	8.7626	-0.1871	76.5	81.5
6	Bwr6.1	81	solcap_snp_sl_14458	SL3.0ch06-39435402	Wilting Score 2019	3.2673	11.0473	-0.1621	78.5	81.5
10	Bwr10.1	53	solcap_snp_sl_33168	SL3.0ch10-63377492	plant width	3.8661	7.6897	-0.1811	50.5	54.5
10	Bwr10.1	53	solcap_snp_sl_33168	SL3.0ch10-63377492	convex width	3.4883	6.8155	-0.1714	50.5	54.5
12	Bwr12.1	37	solcap_snp_sl_1525	solcap_snp_sl_1572	CM height	4.1755	10.7222	0.1837	33.5	40.5
12	Bwr12.2	42	solcap_snp_sl_58807	solcap_snp_sl_9707	Y mass	3.3249	8.5939	0.1651	40.5	43.5

Table 2 Overview of the 20 wilting QTL identified in 10 clusters across the tomato genome at 6 dpi. LOD: maximum value of the Logarithm of the odd. PVE: Percentage of phenotypic variance explained. Add: Additive effect. Left CI and Right CI are the confidence interval calculated by a one-LOD decrease from the estimated QTL position.

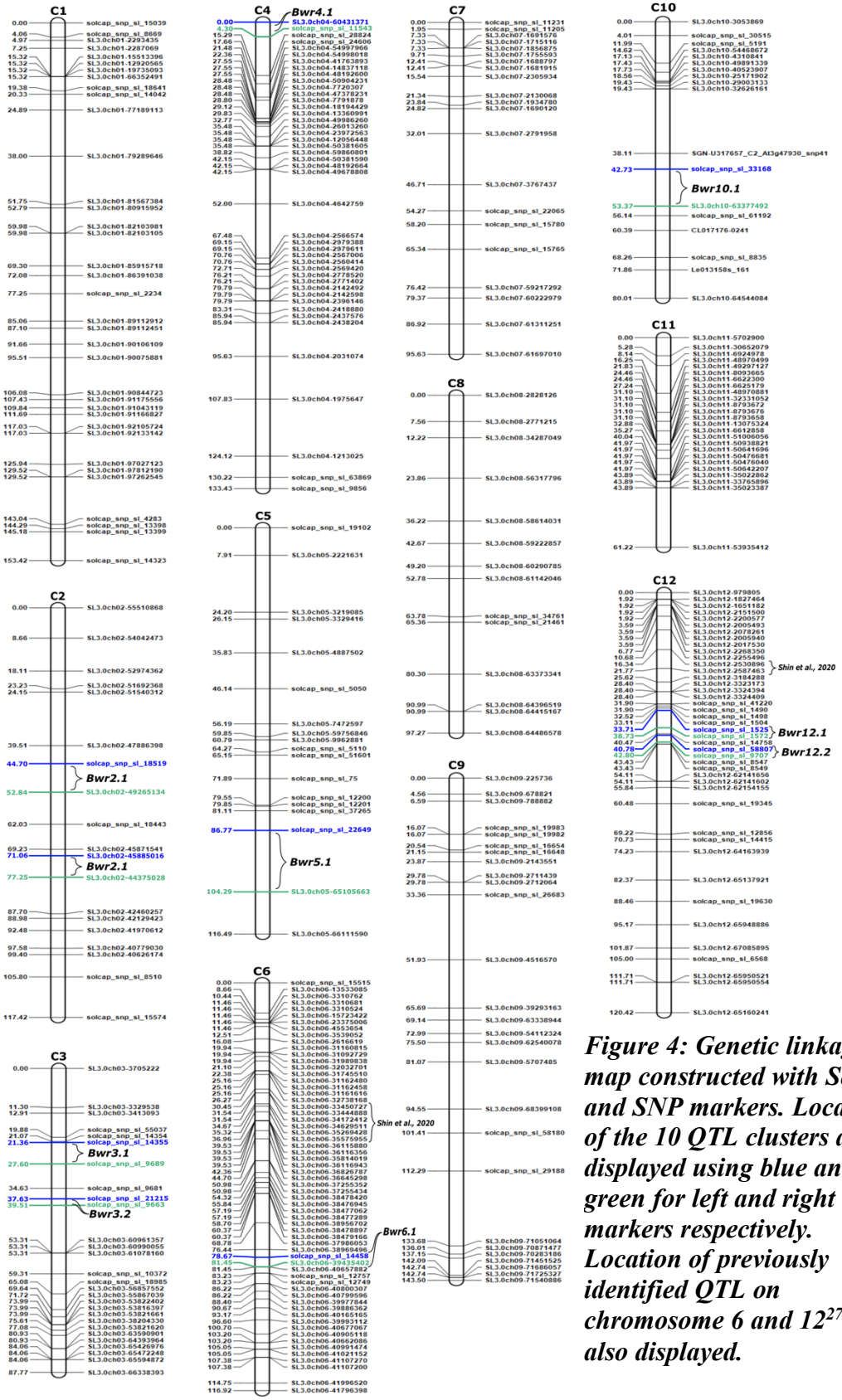

Figure 4: Genetic linkage map constructed with SolCap and SNP markers. Location of the 10 QTL clusters are displayed using blue and green for left and right markers respectively. Location of previously identified QTL on chromosome 6 and 12[27] are also displayed.

165 The parent that donated the favorable allele was determined according to the sign of the QTL
166 additive effect [30], where a positive sign referred to H7996 resistant parent and a negative sign to
167 WV susceptible parent. Typically, in QTL analysis the favorable allele has the higher trait value.
168 Here, a higher trait value is favorable in all cases except the visual wilting score, in which a
169 higher trait value was associated with susceptibility (e.g. 90% wilting is more susceptible than
170 20% wilting). For QTL detected using our visual wilting score, the susceptibility allele was
171 contributed by the susceptible parent WV (Table 2), consistent with other tomato-*R.*
172 *solanacearum* QTL studies based on visual assessment of wilting. For all QTL except those on
173 chromosome 2 and 10, the favorable allele was contributed by Hawaii 7996. QTL clusters on
174 chromosome 2 and 10, which contributed to plant height and width, were donated by the
175 susceptible parent WV. Favorable allelic contribution from both resistant and susceptible parents
176 is common in QTL studies for resistance [30,31].
177
178 Among the 20 individual *Bwr* QTL were 10 QTL clusters (Table 2). We use the term 'QTL
179 cluster' to describe QTL for different traits that co-localize at the same left and right genetic
180 marker. There are between one and six *Bwr* QTL within a given cluster, and each QTL within
181 the cluster has different LOD scores and explains a different percentage of phenotypic variation.
182 Together the clusters explained more than 88% of the variation (calculated using the sum of the
183 QTL with the highest PVE in each cluster).
184
185 *Bwr* QTL for traits that are highly correlated with each other (Figure 3) tended to cluster
186 together. For example, a cluster of QTL on chromosome 3 (*Bwr3.1*; Table 2) contains six *Bwr*
187 QTL, including three for area-related traits (convex width, and X mass and CM width), which

188 are correlated with each other at r = 0.94 - 0.97 (Figure 3). In another cluster (*Bwr3.2*) on this
189 same chromosome, *Bwr* QTL for traits that describe plant area were detected together. This co-
190 localization supports the robust nature of our analyses.
191
192 In other clusters, only one trait that described one aspect of the wilting phenotype was present.
193 For example, despite several metrics that describe width, only convex width was identified as a
194 QTL on chromosome 4 (*Bwr4.1*; LOD 3.18; PVE = 6%). This suggests that the image-based
195 phenotyping captured genetic variation that is specific to each trait.
196
197 *Image-based phenotyping identifies three types of QTL clusters*
198 Among our *Bwr* QTL clusters, we identified three types: those found using both image-based
199 and visual phenotyping (1 cluster, *Bwr3.2*), those found only through visual phenotyping (1
200 cluster, *Bwr6.1*), and those that were identified only through image-based phenotyping (8
201 clusters; Table 2 and Figure 5).
202
203 For the cluster including both image-based and visual phenotyping, (*Bwr3.2*) on chromosome 3,
204 we detected QTL for convex area, plant area and visual plant wilting in 2016 (Table 2 and Figure
205 5a). Previous studies examining tomato responses to other strains of *Ralstonia* have not detected
206 *Bwr* QTL in this region, indicating that it may be a novel target for *R. solanacearum* strain K60.
207 The identification of both image-based and visual QTL within the same cluster suggests that our
208 phenotyping methods are robust at identifying features of plant wilting. Close to this cluster is
209 *Bwr3.1*, which detected QTL for traits based on plant width, including convex width and CM

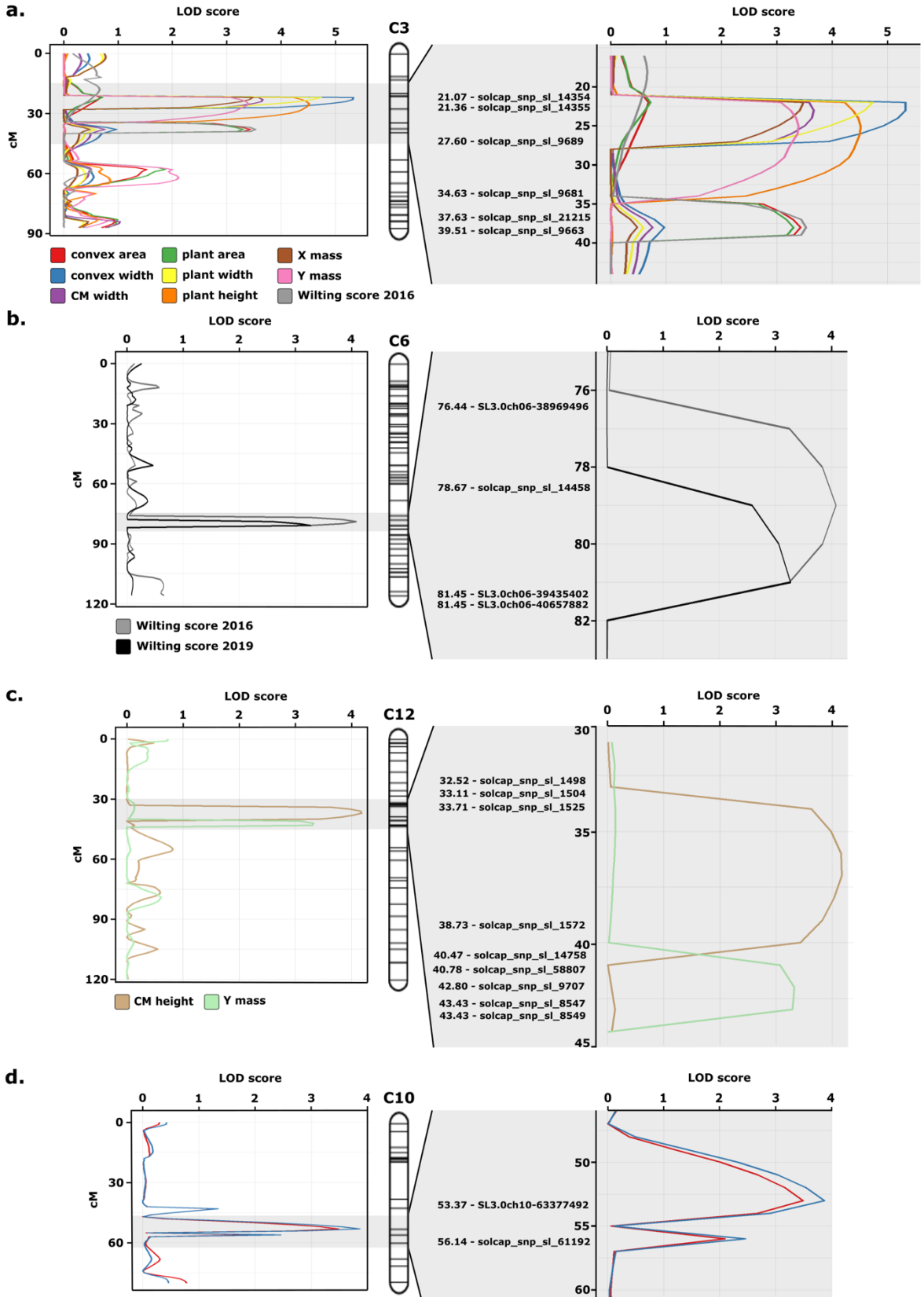

Figure 5: Significant QTL clusters on chromosomes 3 (a.), 6 (b.), 12 (c.) and 10 (d.). The image-based and visually assessed traits are represented with different colors for each chromosome. The vertical axis represents the genetic position (cM) and horizontal axis shows the LOD score. For each chromosome, the left panel represents the entire chromosome and the right panel represents the significant QTL cluster regions.

211 width. The proximal arm of chromosome 3 may be an important but unexploited region for
212 defense against *R. solanacearum* strain K60.
213
214 On chromosome 6 we detected *Bwr* (*Bwr6.1*) using only visual assessment for both 2016 and
215 2019 (Table 2, Figure 5b). This region may be a 'hot spot' for QTL for resistance to multiple
216 strains of *Ralstonia*. Previous studies using this same tomato population for mapping *Bwr* to
217 other strains of *Ralstonia* detected QTL approximately 4 Mb from this position (Figure 4).
218
219 In all other clusters, QTL were identified using only image-based phenotyping. Two such
220 clusters, detected on chromosome 12, identified QTL for CM height (*Bwr12.1*) and Y mass
221 (*Bwr12.2*), and were located near previous QTL detected against other strains of *Ralstonia*
222 (Figure 4 and Figure 5c) . These previous studies [24,26,27] detected QTL using visual wilt
223 assessment of adult plants in the field.
224
225 The remaining QTL detected through image-based phenotyping have not been previously
226 identified in studies using other strains of *Ralstonia*. These regions may be effective only against
227 specific strains of *Ralstonia* ('strain-specific' QTL), or may include those that are not easily
228 detected using visual assessment. In support of the latter, at one of the image-based-only clusters,
229 *Bwr10.1* (Figure 5d), we detected a QTL using visual assessment that did not meet our threshold
230 for significance after permutation (Supplementary Table 2). Thus, image-based phenotyping
231 improved our ability to detect QTL.
232
233 *Image-based phenotyping identified Bwr QTL prior to visual symptom development*

234 In our system, wilting symptoms begin to appear on highly susceptible plants at 4 dpi, and these
235 plants are nearly 100% wilted by 6 dpi. To test whether we could detect *Bwr* QTL prior to the
236 onset of visual symptoms, we performed QTL analysis at 3, 4 and 5 dpi. No QTL were identified
237 based on visual assessment at any of these time points, however several QTL were identified
238 based on image-based phenotyping. At 3 dpi, three clusters were detected on chromosome 3, two
239 of which co-localized with those identified at 6 dpi (Table 3). *Bwr3.1*, a cluster detected only by
240 image-based phenotyping, and *Bwr3.2*, a cluster detected by both visual and image-based
241 phenotyping, were first detected at 3 dpi. *Bwr3.1* was also detected at 5 and 6 dpi, while *Bwr3.2*
242 was detected 3, 4, 5 and 6 dpi (Table 3). A small number of additional QTL were detected at

Clusters	Position	LeftMarker	RightMarker	Timepoint	TraitName	LOD	PVE	Add	LeftCI	RightCI
Bwr3.1	25	solcap_snp_sl_14355	solcap_snp_sl_9689	3	CM height	7.2477	18.2665	0.2584	21.5	30.5
Bwr3.1	27	solcap_snp_sl_14355	solcap_snp_sl_9689	3	CM width	3.5022	8.8528	0.1536	22.5	32.5
Bwr3.1	26	solcap_snp_sl_14355	solcap_snp_sl_9689	3	plant width	5.5180	13.9255	0.2191	21.5	27.5
Bwr3.1	26	solcap_snp_sl_14355	solcap_snp_sl_9689	3	X mass	4.5407	11.7470	0.1991	22.5	32.5
Bwr3.1	22	solcap_snp_sl_14355	solcap_snp_sl_9689	5	CM height	3.6770	9.3886	0.1414	21.5	27.5
Bwr3.1	22	solcap_snp_sl_14355	solcap_snp_sl_9689	5	plant width	3.4953	9.3017	0.1806	21.5	27.5
Bwr3.1	25	solcap_snp_sl_14355	solcap_snp_sl_9689	5	plant height	3.6851	8.5381	0.1738	21.5	31.5
Bwr3.1	25	solcap_snp_sl_14355	solcap_snp_sl_9689	5	Y mass	3.4687	9.9830	0.1673	21.5	31.5
Bwr3.1	22	solcap_snp_sl_14355	solcap_snp_sl_9689	6	convex width	5.3238	10.2506	0.2103	21.5	26.5
Bwr3.1	22	solcap_snp_sl_14355	solcap_snp_sl_9689	6	plant width	4.7309	9.1511	0.1976	21.5	25.5
Bwr3.1	25	solcap_snp_sl_14355	solcap_snp_sl_9689	6	plant height	4.5107	7.6902	0.1896	21.5	31.5
Bwr3.1	23	solcap_snp_sl_14355	solcap_snp_sl_9689	6	CM width	3.6627	6.2716	0.1887	21.5	27.5
Bwr3.1	22	solcap_snp_sl_14355	solcap_snp_sl_9689	6	X mass	3.4765	5.8012	0.1705	21.5	26.5
Bwr3.1	25	solcap_snp_sl_14355	solcap_snp_sl_9689	6	Y mass	3.3918	9.3283	0.1708	21.5	31.5
Bwr3.2	39	solcap_snp_sl_21215	solcap_snp_sl_9663	3	convex width	5.6025	13.8198	0.2120	37.5	42.5
Bwr3.2	39	solcap_snp_sl_21215	solcap_snp_sl_9663	4	convex width	3.9750	10.2036	0.1829	37.5	43.5
Bwr3.2	39	solcap_snp_sl_21215	solcap_snp_sl_9663	4	CM width	4.5294	8.4260	0.1853	37.5	43.5
Bwr3.2	39	solcap_snp_sl_21215	solcap_snp_sl_9663	4	plant width	3.8768	9.9017	0.1838	37.5	43.5
Bwr3.2	39	solcap_snp_sl_21215	solcap_snp_sl_9663	4	X mass	3.8156	9.7282	0.1837	37.5	43.5
Bwr3.2	39	solcap_snp_sl_21215	solcap_snp_sl_9663	5	convex width	3.7859	9.8306	0.1891	37.5	43.5
Bwr3.2	39	solcap_snp_sl_21215	solcap_snp_sl_9663	5	CM width	4.0630	7.4955	0.1924	35.5	39.5
Bwr3.2	38	solcap_snp_sl_21215	solcap_snp_sl_9663	6	Wilting Score 2016	3.5258	7.3736	-0.1726	35.5	39.5
Bwr3.2	38	solcap_snp_sl_21215	solcap_snp_sl_9663	6	convex area	3.4328	9.0796	0.1953	34.5	39.5
Bwr3.2	38	solcap_snp_sl_21215	solcap_snp_sl_9663	6	plant area	3.3019	8.6697	0.1902	34.5	39.5

Table 3 Overview of the QTLs Bwr3.1 and Bwr3.2 identified on chromosome 3 at 3, 4, 5 and 6 dpi by image-based and visually assessed traits.

243 earlier time points (Supplementary Table 3), but in most cases these were not stable, since they
244 were not present at 6 dpi. These data suggest that image-based phenotyping can identify *Bwr*
245 QTL prior to the onset of wilting symptoms.
246
247 *Plant architecture QTL do not overlap with Bwr QTL*
248 The parents of the RIL population, H7996 and WV, have different aboveground phenotypes
249 (Supplementary Figure 4) and the shoot architecture of the RILs correspondingly varies. To
250 ensure that *Bwr* QTL were the result of tomato responses to *Ralstonia*, and not due to differences
251 in aboveground plant architecture, we used our traits in a QTL analysis at -1 dpi, the day before
252 plants had been inoculated. We call these 'tomato plant architecture (*Tpa*)' QTL. We identified
253 16 *Tpa*, within 9 QTL clusters (Table 4). None of the 16 *Tpa* were detected within the same
254 interval as *Bwr* at 6 dpi. However, two *Tpa* QTL clusters were detected that were near *Bwr* QTL
255 present at 6 dpi. One of these was detected on chromosome 3 at position 30, between *Bwr3.1* and
256 *3.2*. While we cannot rule out the possibility that the same genes underlie these *Tpa* and *Bwr*

Chromosome	Cluster	Position	LeftMarker	RightMarker	TraitName	LOD	PVE	Add	LeftCI
2	Tpa2.1	117	solcap_snp_sl_8510	solcap_snp_sl_15574	plant width	3.3851	6.4842	0.129	114.5
2	Tpa2.1	117	solcap_snp_sl_8510	solcap_snp_sl_15574	X mass	4.1424	6.8279	0.139	114.5
3	Tpa3.1	30	solcap_snp_sl_9689	solcap_snp_sl_9681	plant area	3.6327	8.0934	0.1522	24.5
3	Tpa3.2	58	SL3.0ch03-61078160	solcap_snp_sl_10372	plant width	3.2538	9.4831	0.1555	56.5
3	Tpa3.2	58	SL3.0ch03-61078160	solcap_snp_sl_10372	X mass	3.8291	9.4218	0.1628	56.5
3	Tpa3.2	59	SL3.0ch03-61078160	solcap_snp_sl_10372	CM height	3.794	3.6957	0.1603	56.5
4	Tpa4.1	128	SL3.0ch04-1213025	solcap_snp_sl_63869	CM height	3.8063	12.0286	-0.2891	127.5
6	Tpa6.1	10	SL3.0ch06-13533085	SL3.0ch06-3310762	convex area	4.741	11.2755	0.1621	8.5
6	Tpa6.1	10	SL3.0ch06-13533085	SL3.0ch06-3310762	plant width	3.5865	6.9265	0.1336	8.5
6	Tpa6.1	10	SL3.0ch06-13533085	SL3.0ch06-3310762	plant area	3.5117	7.3344	0.1457	8.5
6	Tpa6.1	10	SL3.0ch06-13533085	SL3.0ch06-3310762	X mass	4.8686	8.016	0.151	8.5
6	Tpa6.1	10	SL3.0ch06-13533085	SL3.0ch06-3310762	Y mass	4.902	9.3612	0.1757	8.5
8	Tpa8.1	80	solcap_snp_sl_21461	SL3.0ch08-63373341	X mass	3.2439	5.3622	0.123	74.5
9	Tpa9.1	36	solcap_snp_sl_26683	SL3.0ch09-4516570	CM height	4.8307	6.146	0.2081	32.5
9	Tpa9.2	67	SL3.0ch09-39293163	SL3.0ch09-63338944	convex area	3.1976	7.523	-0.1323	60.5
10	Tpa10.1	71	solcap_snp_sl_8835	Le013158s_161	Y mass	3.2077	5.9734	0.1404	68.5

Table 4 Overview of tomato plant architecture (Tpa) QTL identified at -1 dpi by image-based phenotyping.

257 QTL, their different marker intervals, coupled with the visual wilting QTL that is within the
258 *Bwr3.2* cluster, suggests that different genes are responsible for these QTL. Together, these data
259 suggest that our image-based phenotyping detected genomic regions that function in responding
260 to *Ralstonia* and *Bwr* QTL are not the result of differential growth patterns within the RILs.
261

262 **Discussion**

263 Breeding for plant disease resistance is one of the best strategies to combat plant diseases and
264 prevent major crop loss, but is challenging in part due to the complicated nature of disease
265 phenotyping. Here we used image-based phenotyping with RGB images to identify 20 QTL in
266 10 clusters for tomato responses to *Ralstonia* at 6 dpi, two of which were detected as early as 3
267 dpi. Together, the 20 *Bwr* QTL at 6 dpi explained more than 88% of the variation in response to
268 *Ralstonia*. Image-based phenotyping for shape-based traits that were correlated with wilting
269 detected both novel loci and those that overlapped with QTL based on human visual assessment.
270 These results establish the importance and feasibility of quantitative imaged-based phenotyping
271 to identify new genetic targets for crop disease resistance.
272

273 *Benefits of image-based phenotyping*

274 Imaged-based phenotyping has been used to detect QTL associated with plant root [32] and shoot
275 [33–35] architecture, plant height [36], salt stress [37], and yield [38,39] among other traits. Although image-
276 based phenotyping has become increasingly common to quantify plant disease symptoms [4–7,11–
277 16], to our knowledge, it has yet to be used in the identification of new genetic loci for disease
278 resistance. One reason may be that many plant disease symptoms often occur at the leaf scale
279 (such as spots and specks), making it difficult to use some sensors in high-throughput or at the

280 proper resolution needed to assess disease. While wilting does occur at the leaf scale, it is an
281 easier phenotype to assess at the whole plant scale. Another possibility is that imaging sensors
282 are often expensive, making it more challenging to phenotype the large number of plants needed
283 in a QTL or GWA study.
284
285 Our image-based phenotyping identified loci that function in tomato responses to *Ralstonia*, but
286 did not detect one of the two *Bwr* clusters (*Bwr6.1*) we found using visual assessment of disease.
287 Visual assessment was performed at 8 dpi, while our image based phenotyping ended at 6 dpi. It
288 is possible *Bwr6.1* is not apparent until very late stages of disease. Alternatively, these results
289 could mean that the visually assessed wilting phenotype relies on human complexity that cannot
290 be broken into individual traits, or that we missed components of wilting in our image-based
291 traits. However, a more likely explanation is that our image-based traits were averaged across
292 eight two dimensional images, but wilting is a three dimensional (3D) phenotype. Images in 3D
293 may allow detection of *Bwr6.1*. It would also be of interest to test whether using additional types
294 of sensors – hyperspectral for example - would identify *Bwr 6.1*. Multi and hyperspectral
295 imaging has been used to detect the chemical changes in disease [12,14,40] and would likely be very
296 useful for quantifying water-stress changes associated with diseases like wilting.
297
298 *New QTL for responses to Ralstonia in tomato*
299 As in tomato, resistance to *Ralstonia* in other Solanaceous crops is quantitative [20–26,41]. Breeding
300 for resistance QTL is thus the primary way forward to developing *Ralstonia*-resistant crops in the
301 Solanaceae. This has not been easy, in part because of the diversity of *Ralstonia*. The *Ralstonia*
302 *solanacearum* species complex was recently subdivided into three species (*R. solanacearum*, *R.*

303 *pseudosolanacearum*, and *R. syzygii*), each prevalent in a different part of the world [42–44]. Each
304 species has multiple strains, with an overlapping, but distinct set of virulence proteins that
305 promote disease [45]. Varieties with effective resistance will likely have QTL that are effective
306 against local strains (strain-specific QTL) as well as those effective against multiple strains
307 (broad-spectrum QTL).
308
309 Most previously identified QTL have focused on resistance to *R. pseudosolanacearum*, and none
310 of them used the strain of *R. solanacearum* as in this work [20–27]. Using visual assessment of
311 wilting and the same RIL population of tomato (H7996 x WV700) used here, one broad-
312 spectrum QTL for resistance to multiple strains of *R. pseudosolanacearum,* and one strain of *R.*
313 *solanacearum* (JT-516) had been previously identified on chromosome 6 [20–27]. We also identified
314 a QTL on chromosome 6, using visual assessment in both 2016 and 2019. In our study, *Bwr6.1*
315 confers 8 – 11% of the variation, compared to 11.5 – 33% for *Bwr6a* - *Bwr6d* [26,27]. The genes
316 within the left and right intervals of *Bwr6.1* are particularly interesting because there are two
317 groups of NBS-LRRs located between the left and right markers for *Bwr6.1*
318 (solcap_snp_sl_14458 and the GBS-identified SNP at 39435402). One of these groups includes
319 the *S. lycopersicum* homolog of Arabidopsis *RESISTANCE to PSEUDOMONAS SYRINGAE 4*
320 (*RPS4*). Fine-mapping of *Bwr6.1* is needed to determine whether a specific NBS-LRR protein or
321 receptor is responsible for the resistance conferred by this region.
322
323 Previous studies also identified a major QTL on chromosome 12 that is effective for resistance to
324 *R. pseudosolanacearum*, and explained between 15.9 – 53.9% of the variation [27]. We found two
325 clusters of QTL on chromosome 12, for image-based traits. Within the region spanning *Bwr12.1*

326 on chromosome 12 is one NBS-LRR disease resistance gene (*Solyc12g10740*) and one receptor-
327 like kinase (*Solyc12g010660*) while within *Bwr12.2* are genes related to disease resistance
328 pathways, including a gene encoding a Pathogenesis Response (PR) Protein (*Solyc12g014310*),
329 and two genes encoding Leucine Rich Repeat – Receptor Like Kinases (*Solyc12g014350* and
330 *Solyc12g150105*). Our results suggest that this region of chromosome 12 may be important for
331 resistance to multiple strains of *Ralstonia*. The QTL we identified on chromosomes 2, 3, 4, 5, 8
332 and 10 were not previously identified, and thus may be specific to *R. solanacearum* strain K60.
333 With the exception of *Bwr3.2*, these QTL were detected using only our image-based traits.
334 Together, our results establish the value of image-based disease phenotyping for uncovering
335 novel genetic components and new targets for quantitative disease resistance in crops. By
336 identifying new genetic loci, this type of phenotyping may enable more broad-spectrum and
337 durable resistance.
338
339 **Methods**
340 ***Plant growth***
341 Seeds of 188 Hawaii7996 (H7996) x West Virginia700 (WV) recombinant inbred lines (RIL) in
342 the F8 generation were obtained from the Asian Vegetable Research and Development Center
343 (AVRDC) in June 2014. Seeds were propagated to the F_9 generation in field and greenhouse in
344 West Lafayette, IN in 2014 and 2015 and were used in QTL analysis in 2016 and 2019.
345
346 For all plants used in the imaging experiments and 2019 visual assessment of wilting, seeds were
347 sown into individually labeled 1801 traditional inserts that were placed into 1020 flats (Hummert
348 International, USA). Seeds in the 2016 experiment were sown into individually labeled 1203

349 inserts that were placed into 1020 flats. Seeds were sown into ProMix Propagation Mix supplied
350 by the Lilly Greenhouses and Growth Facility located at Purdue University, West Lafayette,
351 Indiana, USA. The individual pots were randomized and placed in a growth chamber at 28ºC,
352 relative humidity of 65% for a lighting cycle of 16 hours light/8 hours dark. The plants began
353 germination on day 4 and plants were inoculated with *R. solanacearum* strain K60 at 17 days
354 after planting when three true leaves were present. Trays were rotated in the growth chamber
355 throughout each experiment. In 2016, four seeds of each RIL were grown in the growth chamber
356 with parental controls, and each plant was visually assessed for wilting at 8 days post inoculation
357 (dpi). In 2019, one seed per RIL, along with parental controls, was grown in the growth chamber
358 for each of five independent replicates. Each plant was imaged at -1, 3, 4, 5, and 6 dpi, and
359 visually assessed at 8 dpi.
360
361 For plants used to genotyping with tomato SolCap markers, F_9 generation RIL seeds and parental
362 controls were grown in the greenhouse in 2-gallon pots with Metro Mix 510 soil. Plants were
363 grown for 6 weeks.
364
365 ***Ralstonia solanacearum growth and plant inoculation***
366 *Ralstonia solanacearum* strain K60 (containing a GFP reporter) was grown on casamino acid-
367 peptone-glucose (CPG) agar containing tetrazolium chloride (TZC) in the dark for 48 hours at
368 28ºC as in [46]. Briefly, bacteria were resuspended in sterile water to a concentration of
369 approximately 2 x 10^8 colony forming units (CFU)/mL for each experiment. For each
370 experiment, the concentration of inoculum was confirmed through dilution plating. Pots of three-

371 leaf plants were lightly compressed to induce wounding similar to transplant handling in field
372 conditions. 60 mL of inoculum was applied to the surrounding soil using a serological pipet.
373
374 ***Visual assessment of bacterial wilt disease***
375 Wilt scores were visually assessed 8 dpi. Wilt scores were calculated by counting the number of
376 wilted true leaves divided by the total number of true leaves on the plant. Plants were scored with
377 a 95% if the plant had all of its leaves wilted, excluding the topmost leaf. Plants were marked as
378 100% when the topmost portion of the stem was collapsed and wilted (Supplementary Figure 2).
379
380 ***Plant imaging***
381 Plants were imaged the day before inoculation (-1 dpi) and then imaged on 3, 4, 5, and 6 dpi. A
382 Linco Linstor 2000-watt photo studio (Amazon, USA) was used as the backdrop, and Flora X
383 fluorescent lighting (Amazon, USA) was used to create a small photo studio. Individual plants
384 were placed on a Photocapture 360 turntable (Ortery Technologies) that was programmed to
385 capture eight images around the plant (every 45°). The images were captured using an EOS 6D
386 Canon camera with an EF 50mm f/1.4 USM lens on a stationary tripod. An imaging carriage
387 was created with a square petri dish and a fiducial marker attached to each side. A total of five
388 independent replicates for each RIL and the parental controls were imaged.
389
390 ***Phenotyping Pipeline and Image Analysis***
391 From the plant images, ten traits were acquired for QTL analysis. A detailed description of the
392 acquisition process can be found in [47,48]. All traits were extracted based on plant color and shape.
393 To eliminate any color discrepancy between images, images were automatically color corrected

using a fiducial marker consisting of a colored checkerboard with known physical dimensions and colors.

After color correction, plant pixels were segmented from the rest of the image by thresholding channels in the L*A*B* color space. The resulting segmentation mask was improved with image morphological operations to fill holes and remove noise generated by the thresholding. The stem of the plant was identified using two neural networks, Mask R-CNN and U-Net. By locating the stem of the plant, metrics were defined that reflect the inner morphology of the plant. To train the neural networks, stem segmentation ground truth data were generated using Adobe Photoshop and LabelMe (a Python-based annotation tool) to mark the location of the image pixels belonging to the stem of the plant. Further details about this procedure are described in [47,48].

The plant and stem masks were used in the subsequent color and shape analysis, which acquired ten traits: total area of the plant mask (plant area), height of the plant mask (plant height), maximum width of the plant mask (plant width), area of the convex hull (convex area), width of the convex hull (convex width), color-based weighted average (color average), horizontal distance between the center of mass of the left and right sides of the plant stem (CM width), height of the center of mass (CM height), x-axis distribution of the center of mass (X mass), Y-axis distribution of the center of mass (Y mass).

The plant area, plant height and plant width were calculated from the plant mask. When calculating plant height, the upper 5% of the plant material was not included, which helped

417 eliminate the impact of small leaves growing at the top. Using functions available in *OpenCV*
418 Python Library, a convex hull was fit around the plant mask and the convex area and convex
419 width were calculated. For color analysis, the weighted average of the pixel values in the A*
420 channel was calculated, as this channel captures the green-magenta spectrum.
421
422 To calculate traits involving the center of mass (CM), the plant mask was split into left and right
423 halves using the stem mask [48], and the CM located for each half. The x-axis distance between
424 CMs (CM width) and the average height of the CMs (CM height) were used as traits.
425
426 The extension of just one leaf can have a major impact on measured plant width, generating a
427 disproportionately larger value. Capturing the plant material distribution inside the plant mask
428 can overcome this issue. Using the split plant mask, the horizontal and vertical distribution of
429 plant material was estimated. The distances at which 90% of the plant material was captured in
430 the horizontal and vertical directions were used as the traits 'X mass distribution' and 'Y mass
431 distribution'. The average of eight views around the plant were used for each trait value.
432
433 In the random forest classification, visual wilting scores were thresholded to 0 or 1, where 0 = 0
434 to 50% wilting, 1 = 51 – 100% wilting. Average trait values from eight views from 6 dpi for 969
435 plants (RILs and parental controls) were used across all five replicates. Some plants did not have
436 a trait value for that day and were not used in the algorithm.
437
438 ***DNA extraction, Marker generation and Genotyping by Sequencing (GBS)***

439 Tomato SolCap markers and single nucleotide polymorphisms (SNPs) identified through GBS
440 were used for map creation. Leaf disc samples were collected from each RIL plant using a
441 biopsy punch and were sent to LGC, Biosearch Technologies. Genomic DNA was extracted and
442 genotyped for 128 SNPs from the Tomato SolCAP panel using LGC's KASP assay. One
443 hundred twelve SNPs were obtained for RILs using this method.
444
445 For GBS, genomic DNA (gDNA) was extracted from 188 F_9 individuals of the RIL population
446 and from parental plants using Trizol. gDNA was RNase-treated and cleaned with phenol
447 chloroform extraction. Sequencing library preparation was as described by [49]. Briefly, gDNA
448 was digested with *PstI* and 150 bp paired end sequencing was performed on two lanes of an
449 Illumina Hi-seq 2500 at the Purdue Genomics Facility.
450
451 Reads were mapped to the *Solanum lycopersicum* 3.0 genome using the methods of [50]. In brief,
452 reads were de-multiplexed, and adapter sequences were removed. Reads were filtered based on
453 the presence of a GBS barcode on the forward read (R1), which accounts for 95.4% of the PE
454 reads. For these R1, 97.3% had a paired R2 read, and 2.7% did not have a pair. R1 read pairs
455 and R1 singles reads were combined and assessed independent of pairing and treated as single
456 end reads for the remaining analyses (924,500,737 reads).
457
458 Reads were filtered to remove those with the presence of an internal restriction site, the lack of
459 restriction site hang sequence at the end, and for minimum length, which retained 93.0% of the
460 reads. There was a minimum of 17,561 reads, a maximum of 16,127,292 reads, and an average
461 of 4,480,149 reads per sample (Supplementary Figure 7). Reads were mapped using BWA-

462 MEM for paired end reads, and the GATK haplotype caller was used to generate a genomic
463 Variant Call Format (gVCF) file for downstream analysis.
464 There were 74,082 SNPs called between the population and *Solanum lycopersicum* 3.0 reference
465 genome. Many of these were SNPs between the reference genome and the population and do not
466 vary in the population used here. Filtering for the presence of two alleles within the RIL
467 population identified resulted in 2,738 SNPs. Of these, the parental alleles were identified in
468 both parents for 278 SNPs and in one parent for 698 SNPs. The remaining 1,762 SNPs could not
469 be assigned a parental origin and were not used for further analysis. The 976 SNPs with parental
470 origin identified were filtered for a minor allele frequency greater than 0.02 and less than 0.99,
471 which resulted in 632 high quality SNPs.
472
473 High quality SNPs identified from GBS were combined with previously defined SolCap markers
474 from LGC Biosearch Technologies for a total of 748 markers. SNP coverage of the 188 RIL taxa
475 was high. Of the 748 markers, the minimum coverage was 115 markers, the maximum coverage
476 was 555 markers, and the average was 366 markers (Supplementary Figure 8a). There was some
477 residual heterozygosity in the taxa (Supplementary Figure 8b), and taxa with 10% or greater
478 heterozygosity were removed from further analysis (2 RILs).
479
480 ***Linkage Map Construction***
481 The software QTL IciMapping [29] (version 4.1) was used for the map construction with all 748
482 markers. Redundant markers were filtered by taxa coverage using a missing rate of 85% and a
483 distortion threshold at 0.001 to obtain a total of 408 markers. The 408 markers without anchor
484 information were assigned to 12 groups based on a LOD score threshold value of 3. After

485 grouping, the markers were ordered using the nearest neighbor algorithm (nnTwoOpt) using the
486 rippling criterion SARF (Sum of Adjacent Recombination Frequencies) with a window size of
487 five markers. After ordering, some markers at the end of the chromosomes were deleted when
488 they were adding an insignificant genetic distance to the chromosome. These markers were
489 identified after splitting the current chromosome in two sub-chromosomes between the longest
490 marker interval. If the shortest sub-chromosome contained more than 20% of the markers before
491 splitting, the two sub-chromosome were re-assembled. Otherwise, the shortest sub-chromosome
492 was deleted.

493 ***QTL detection***

494 QTL were detected using Inclusive Composite Interval Mapping with additive effects (ICIM-
495 ADD) in IciMapping [29] (version 4.1) using a genetic mapping with a 1 cM scanning step and a
496 probability in stepwise regression of 0.001. The LOD significance threshold to declare a QTL
497 significant was determined using a Type-I error of 0.0500 after one thousand permutation. For
498 the QTL analysis, we removed 19 of the 188 RIL (10%) showing the highest variation according
499 to the visual wilting score and 3 RIL due to missing data across the 5 biological repetitions for a
500 total of 166 RIL into the QTL map (Supplementary Figure 3). The evolution of the ten image-
501 based traits and two visual wilting scores between -1 dpi and 3, 4, 5 and 6 dpi were determined
502 for the 166 RIL. To assure a normal distribution of the phenotypic data, the function
503 "orderNorm" was used to perform an ordered quantile normalization [51] before QTL analysis
504 using the package "bestNormalize" version 1.6.1 with R software version 3.6.1 [52].

505

506

507 **References**
508

509 1. Colwell, R. N. Determining the prevalence of certain cereal crop diseases by means of aerial
510 photography. *Hilgardia* **26**, 223–286 (1956).
511 2. Jackson, R. D. Remote Sensing of Biotic and Abiotic Plant Stress. *Annu. Rev. Phytopathol.*
512 **24**, 265–287 (1986).
513 3. Bock, C., Poole, G., Parker, P. & Gottwald, T. R. Plant Disease Severity Estimated Visually,
514 by Digital Photography and Image Analysis, and by Hyperspectral Imaging. *Crit. Rev. Plant*
515 *Sci.* **29**, 59-107. (2010).
516 4. Simko, I., Jimenez-Berni, J. A. & Sirault, X. R. R. Phenomic Approaches and Tools for
517 Phytopathologists. *Phytopathology* **107**, 6–17 (2017).
518 5. Shakoor, N., Lee, S. & Mockler, T. C. High throughput phenotyping to accelerate crop
519 breeding and monitoring of diseases in the field. *Curr. Opin. Plant Biol.* **38**, 184–192 (2017).
520 6. Mochida, K. *et al.* Computer vision-based phenotyping for improvement of plant
521 productivity: a machine learning perspective. *GigaScience* **8**, (2019).
522 7. Mir, R. R., Reynolds, M., Pinto, F., Khan, M. A. & Bhat, M. A. High-throughput
523 phenotyping for crop improvement in the genomics era. *Plant Sci.* **282**, 60–72 (2019).
524 8. Bock, C., Parker, P., Cook, A. Z. & Gottwald, T. Visual Rating and the Use of Image
525 Analysis for Assessing Different Symptoms of Citrus Canker on Grapefruit Leaves. *Plant*
526 *Dis.* **92**, 530 - 541 (2008).
527 9. Stewart, E. & McDonald, B. Measuring quantitative virulence in the wheat pathogen
528 *Zymoseptoria tritici* using high-throughput automated image analysis. *Phytopathology* **104**,
529 985 -992 (2014).

10. Stewart, E. L. *et al.* An Improved Method for Measuring Quantitative Resistance to the Wheat Pathogen *Zymoseptoria tritici* Using High-Throughput Automated Image Analysis. *Phytopathology* **106**, 782–788 (2016).
11. Mahlein, A.-K. Plant Disease Detection by Imaging Sensors - Parallels and Specific Demands for Precision Agriculture and Plant Phenotyping. *Plant Dis.* **100**, 241 - 251 (2016).
12. Mahlein, A.-K. *et al.* Plant disease detection by hyperspectral imaging: from the lab to the field. *Adv. Anim. Biosci.* **8,** 238-243 (2017).
13. Mahlein, A.-K. *et al.* Comparison and Combination of Thermal, Fluorescence, and Hyperspectral Imaging for Monitoring Fusarium Head Blight of Wheat on Spikelet Scale. *Sensors* **19**, 2281 (2019).
14. Lowe, A., Harrison, N. & French, A. P. Hyperspectral image analysis techniques for the detection and classification of the early onset of plant disease and stress. *Plant Methods* **13**, 80 (2017).
15. Pérez-Bueno, M. L., Pineda, M. & Barón, M. Phenotyping Plant Responses to Biotic Stress by Chlorophyll Fluorescence Imaging. *Front. Plant Sci.* **10**, (2019).
16. Pineda, M., Barón, M. & Pérez-Bueno, M.-L. Thermal Imaging for Plant Stress Detection and Phenotyping. *Remote Sensing* **13**, 68 (2021).
17. Mansfield, J. *et al.* Top 10 plant pathogenic bacteria in molecular plant pathology. *Mol. Plant Pathol.* **13**, 614–629 (2012).
18. Genin, S. Molecular traits controlling host range and adaptation to plants in Ralstonia solanacearum. *New Phytol.* **187**, 920–928 (2010).
19. Genin, S. & Denny, T. P. Pathogenomics of the *Ralstonia solanacearum* Species Complex. *Annu. Rev. Phytopathol.* **50**, 67–89 (2011).

553 20. Danesh, D., Aarons, S., McGill, G. E. & Young, N. D. Genetic Dissection of Oligogenic
554 Resistance to Bacterial Wilt in Tomato. *Mol. Plant Microbe Interact.* **7**, 464–471 (1994).
555 21. Thoquet, P. *et al.* Quantitative trait loci determining resistance to bacterial wilt in tomato
556 cultivar Hawaii7996. *Mol. Plant Microbe Interact.* **9**, 826–836 (1996).
557 22. Thoquet, P. *et al.* Polygenic resistance of tomato plants to bacterial wilt in the French West
558 Indies. *Mol. Plant Microbe Interact.* **9**, 837–842 (1996).
559 23. Mangin, B., Thoquet, P., Olivier, J. & Grimsley, N. H. Temporal and multiple quantitative
560 trait loci analyses of resistance to bacterial wilt in tomato permit the resolution of linked loci.
561 *Genetics* **151**, 1165–1172 (1999).
562 24. Wang, J. F. *et al.* Resistance of tomato line Hawaii7996 to *Ralstonia solanacearum* Pss4 in
563 Taiwan is controlled mainly by a major strain-specific locus. *Mol. Plant Microbe Interact.*
564 **13**, 6–13 (2000).
565 25. Carmeille, A. *et al.* Identification of QTLs for *Ralstonia solanacearum* race 3-phylotype II
566 resistance in tomato. *Theor. Appl. Genet.* **113**, 110–21 (2006).
567 26. Wang J-W. *et al.* Identification of major QTLs associated with stable resistance of tomato
568 cultivar 'Hawaii 7996' to *Ralstonia solanacearum*. *Euphytica* **190**, 241–252 (2013).
569 27. Shin, I. S. *et al.* Construction of a single nucleotide polymorphism marker based QTL map
570 and validation of resistance loci to bacterial wilt caused by *Ralstonia solanacearum* species
571 complex in tomato. *Euphytica* **216**, 54 (2020).
572 28. Schandry, N. A Practical Guide to Visualization and Statistical Analysis of *R. solanacearum*
573 Infection Data Using R. *Front. Plant Sci.* **8**, (2017).

574 29. Meng, L., Li, H., Zhang, L. & Wang, J. QTL IciMapping: Integrated software for genetic
575 linkage map construction and quantitative trait locus mapping in biparental populations.
576 *Crop J.* **3**, 269–283 (2015).
577 30. Awata, L. A. O. *et al.* Genetic Analysis of QTL for Resistance to Maize Lethal Necrosis in
578 Multiple Mapping Populations. *Genes* **11**, 32 (2020).
579 31. Maschietto, V. *et al.* QTL mapping and candidate genes for resistance to Fusarium ear rot
580 and fumonisin contamination in maize. *BMC Plant Biol.* **17**, 20 (2017).
581 32. Topp, C. N. *et al.* 3D phenotyping and quantitative trait locus mapping identify core regions
582 of the rice genome controlling root architecture. *Proc. Natl. Acad. Sci. U.S.A.* **110**, E1695-
583 1704 (2013).
584 33. Zhang, X. *et al.* High-Throughput Phenotyping and QTL Mapping Reveals the Genetic
585 Architecture of Maize Plant Growth. *Plant Physiol.* **173**, 1554–1564 (2017).
586 34. Knoch, D. *et al.* Strong temporal dynamics of QTL action on plant growth progression
587 revealed through high-throughput phenotyping in canola. *Plant Biotechnology Journal* **18**,
588 68–82 (2020).
589 35. Li, H. *et al.* High-throughput phenotyping accelerates the dissection of the dynamic genetic
590 architecture of plant growth and yield improvement in rapeseed. *Plant Biotechnol. J.* **18**,
591 2345–2353 (2020).
592 36. Wang, X. *et al.* Dynamic plant height QTL revealed in maize through remote sensing
593 phenotyping using a high-throughput unmanned aerial vehicle (UAV). *Sci. Rep.* **9**, 3458
594 (2019).
595 37. Awlia, M. *et al.* Genetic mapping of the early responses to salt stress in *Arabidopsis*
596 *thaliana*. *Plant J.* doi:10.1111/tpj.15310 (2021).

597 38. Tanger, P. *et al.* Field-based high throughput phenotyping rapidly identifies genomic regions
598 controlling yield components in rice. *Sci. Rep.* **7**, 42839 (2017).
599 39. Pauli, D. *et al.* Field-Based High-Throughput Plant Phenotyping Reveals the Temporal
600 Patterns of Quantitative Trait Loci Associated with Stress-Responsive Traits in Cotton. *G3*
601 *Genes Genom. Genet.* **6**, 865–879 (2016).
602 40. Zhang, N. *et al.* A Review of Advanced Technologies and Development for Hyperspectral-
603 Based Plant Disease Detection in the Past Three Decades. *Remote Sens.* **12**, 3188 (2020).
604 41. Young, N. D. & Danesh, D. Understanding Bacterial Wilt Resistance in Tomato through the
605 Use of DNA Genetic-Markers. In: *Bacterial Wilt*: *the disease and its causative agent,*
606 *Pseudomonas solanacearum*, CAB International, Wallingford, 145–155 (1994).
607 42. Remenant, B. *et al.* Sequencing of K60, Type Strain of the Major Plant Pathogen *Ralstonia*
608 *solanacearum*. *J Bacteriol* **194**, 2742–2743 (2012).
609 43. Safni, I. *et al.* Polyphasic taxonomic revision of the *Ralstonia solanacearum* species
610 complex: proposal to emend the descriptions of *Ralstonia solanacearum* and *Ralstonia*
611 *syzygii* and reclassify current *R. syzygii* strains as *Ralstonia syzygii* subsp. *syzygii* subsp.
612 nov., *R. solanacearum* phylotype IV strains as *Ralstonia syzygii* subsp. *indonesiensis* subsp.
613 nov., banana blood disease bacterium strains as *Ralstonia syzygii* subsp. *celebesensis* subsp.
614 nov. and *R. solanacearum* phylotype I and III strains as *Ralstonia pseudosolanacearum* sp.
615 nov. *Int. J. Syst. Evol. Micr.* **64**, 3087–3103.
616 44. Prior, P. *et al.* Genomic and proteomic evidence supporting the division of the plant
617 pathogen *Ralstonia solanacearum* into three species. *BMC Genomics* **17**, 90 (2016).

618 45. Landry, D., González-Fuente, M., Deslandes, L. & Peeters, N. The large, diverse, and robust
619 arsenal of *Ralstonia solanacearum* type III effectors and their *in planta* functions. *Mol. Plant*
620 *Pathol.* (2020) doi:10.1111/mpp.12977.
621 46. Caldwell, D., Kim, B.-S. & Iyer-Pascuzzi, A. S. *Ralstonia solanacearum* Differentially
622 Colonizes Roots of Resistant and Susceptible Tomato Plants. *Phytopathology* **107**, 528–536
623 (2017).
624 47. Yang, C. *et al.* Image-Based Plant Wilting Estimation. *arXiv:2105.12926 [cs]* (2021).
625 48. Yang, C. *et al.* Plant Stem Segmentation Using Fast Ground Truth Generation. *2020 IEEE*
626 *Southwest Symposium on Image Analysis and Interpretation (SSIAI)* 62–65 (2020).
627 49. Elshire, R. J. *et al.* A Robust, Simple Genotyping-by-Sequencing (GBS) Approach for High
628 Diversity Species. *PLOS ONE* **6**, e19379 (2011).
629 50. Manching, H. *et al.* Phased Genotyping-by-Sequencing Enhances Analysis of Genetic
630 Diversity and Reveals Divergent Copy Number Variants in Maize. *G3 Genes Genom. Genet*
631 **7**, 2161–2170 (2017).
632 51. Peterson, R. A. & Cavanaugh, J. E. Ordered quantile normalization: a semiparametric
633 transformation built for the cross-validation era. *J. Appl. Stat.* **47**, 2312–2327 (2020).
634 52. R Core Team. R: A language and environment for statistical computing. *R Foundation for*
635 *Statistical Computing* **Vienna**, URL https://www.R-project.org/.
636

637 **Acknowledgements**

638 We thank Chloe Caldwell for help with imaging, and Kristina Gans for help with GBS.

This work was funded by a Purdue Seed Grant to AIP and ED, a Foundation for Food and Agriculture Research New Innovator Award to AIP, and the endowment of the Charles William Harrison Distinguished Professorship at Purdue University to ED.

Author Contributions

A.I.P. and E.D. designed the study and coordinated the project; V.M., D.C., and B.K. performed experiments; E.E. carried out the GBS analysis; V.M. conducted the QTL analysis; V.M, D.C, A.I.P., S.B., C.Y., and E.D. developed image descriptors; S.B. and C.Y. conducted the image analysis; A.I.P. and V.M. wrote the manuscript; all authors edited the manuscript.

Supplementary Information

Supplementary Figures

Supplementary Figure 1: Design of our low cost phenotyping platform including automatic turntable, backdrop, lightning and RGB camera.

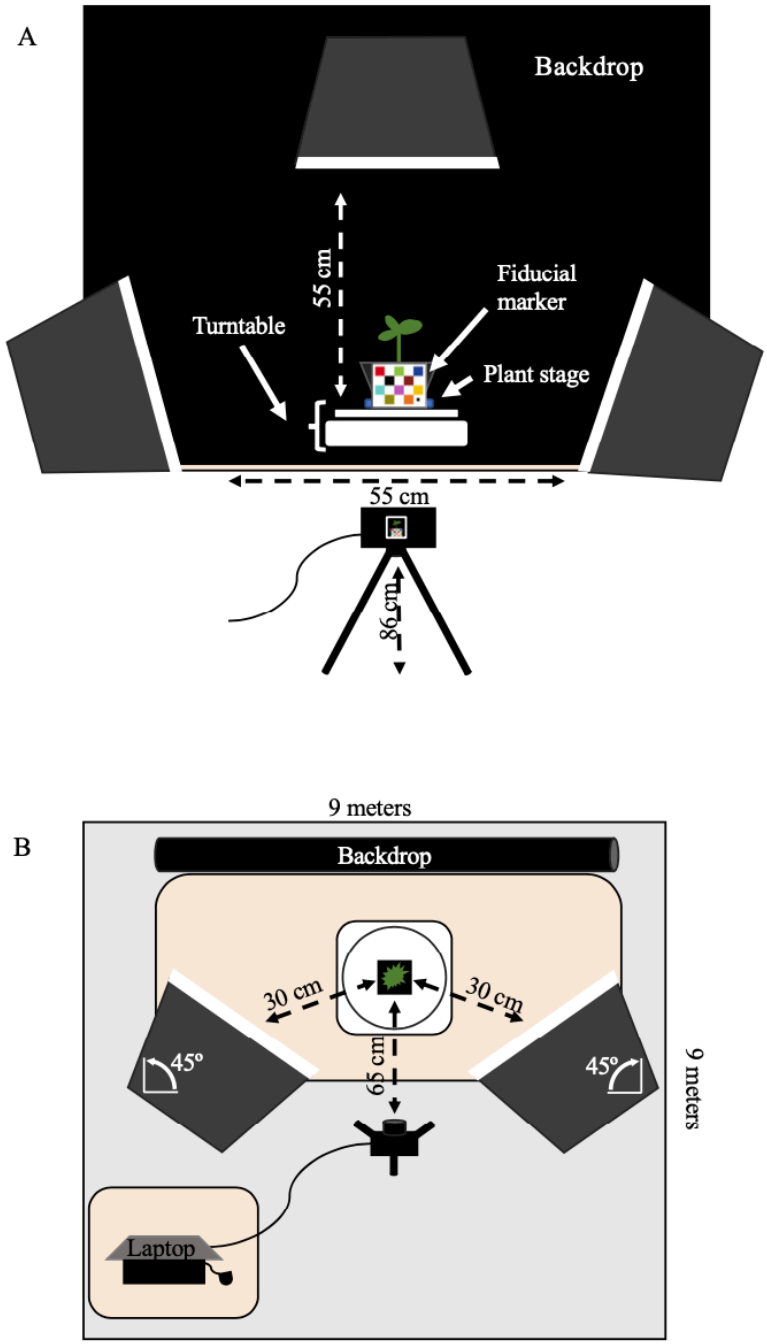

Supplementary Figure 2: Raw RGB pictures showing the evolution of wilting symptoms on RIL # 646 at -1, 3, 4, 5 and 6 dpi. Visually assessed wilting score are expressed in percentage of wilted leaves.

Supplementary Figure 3: Wilting Score RIL: Boxplots showing the normalized wilting score at 6 dpi for the 166 RILs, resistant Hawaii 7996 (HA) and susceptible West Virginia (WV) genotypes.

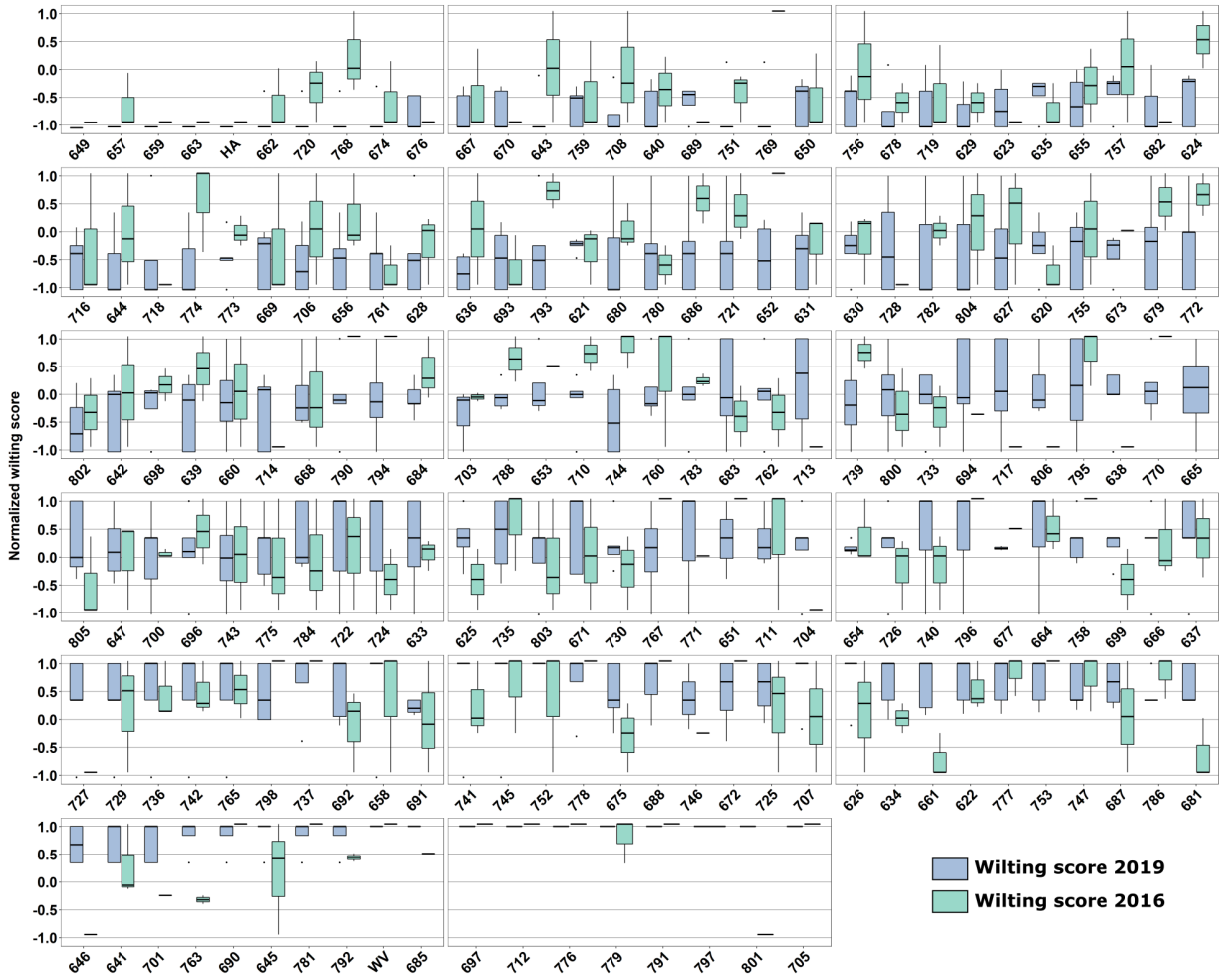

Supplementary Figure 4: RGB pictures showing the evolution of the traits at -1, 3, 4, 5 and 6 dpi for A) Hawaii 7996 and B) West Virginia (pw: plant width, ph: plant height, CMh: Center of Mass height, CMw: Center of Mass width, xm: Horizontal mass distribution, ym: Vertical mass distribution).

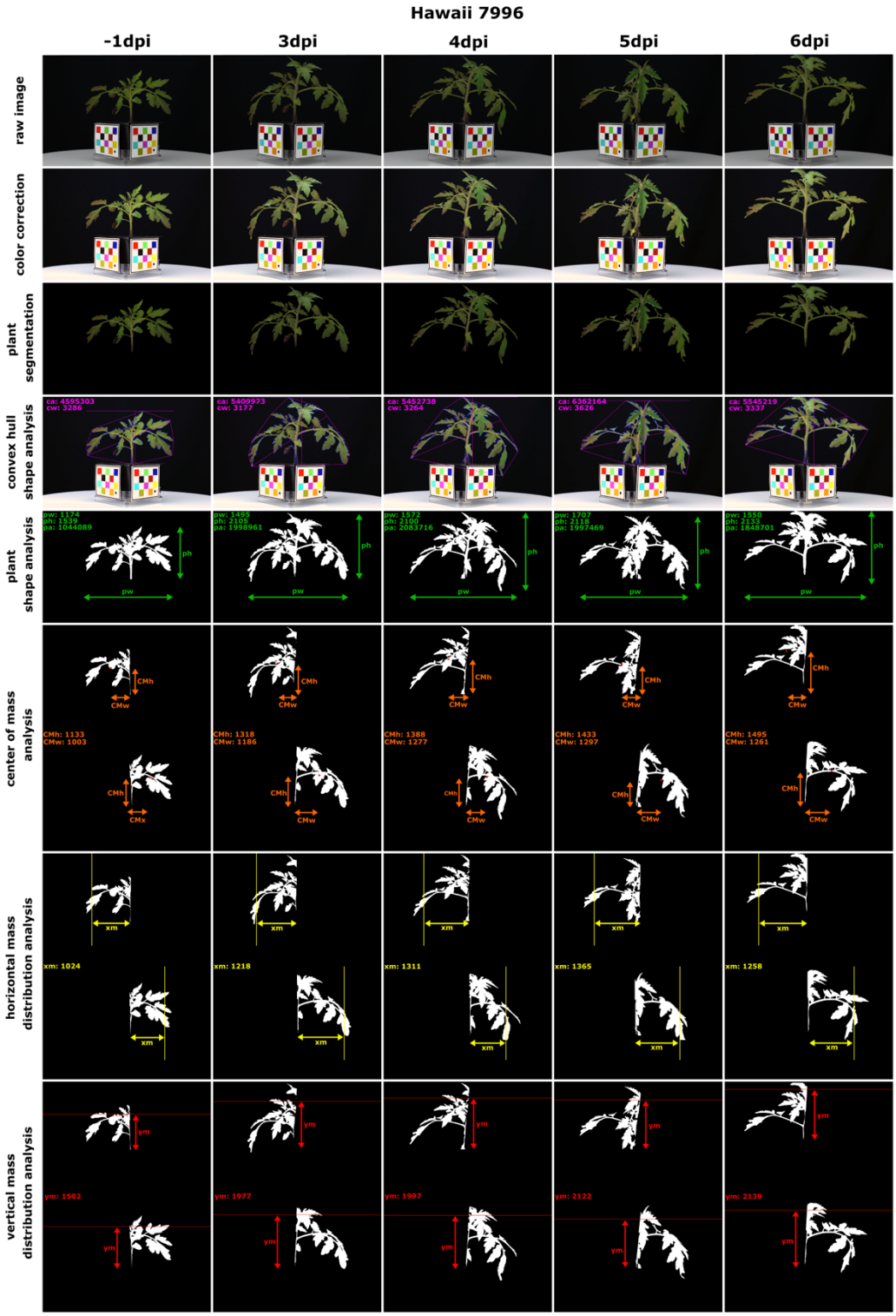
Hawaii 7996
-1dpi
3dpi
4dpi
5dpi
6dpi
raw image
color correction
plant segmentation
convex hull shape analysis
ca: 4595303
cw: 3286
ca: 5409973
cw: 3177
ca: 5452738
cw: 3264
ca: 6362164
cw: 3626
ca: 5545219
cw: 3337
plant shape analysis
pw: 1174
ph: 1539
pa: 1044089
pw: 1495
ph: 2105
pa: 1998961
pw: 1572
ph: 2100
pa: 2083716
pw: 1707
ph: 2118
pa: 1997469
pw: 1550
ph: 2133
pa: 1848701
ph
pw
center of mass analysis
CMh
CMw
CMx
CMh: 1133
CMw: 1003
CMh: 1318
CMw: 1186
CMh: 1388
CMw: 1277
CMh: 1433
CMw: 1297
CMh: 1495
CMw: 1261
horizontal mass distribution analysis
xm
xm: 1024
xm: 1218
xm: 1311
xm: 1365
xm: 1258
vertical mass distribution analysis
ym
ym: 1502
ym: 1977
ym: 1997
ym: 2122
ym: 2139

703

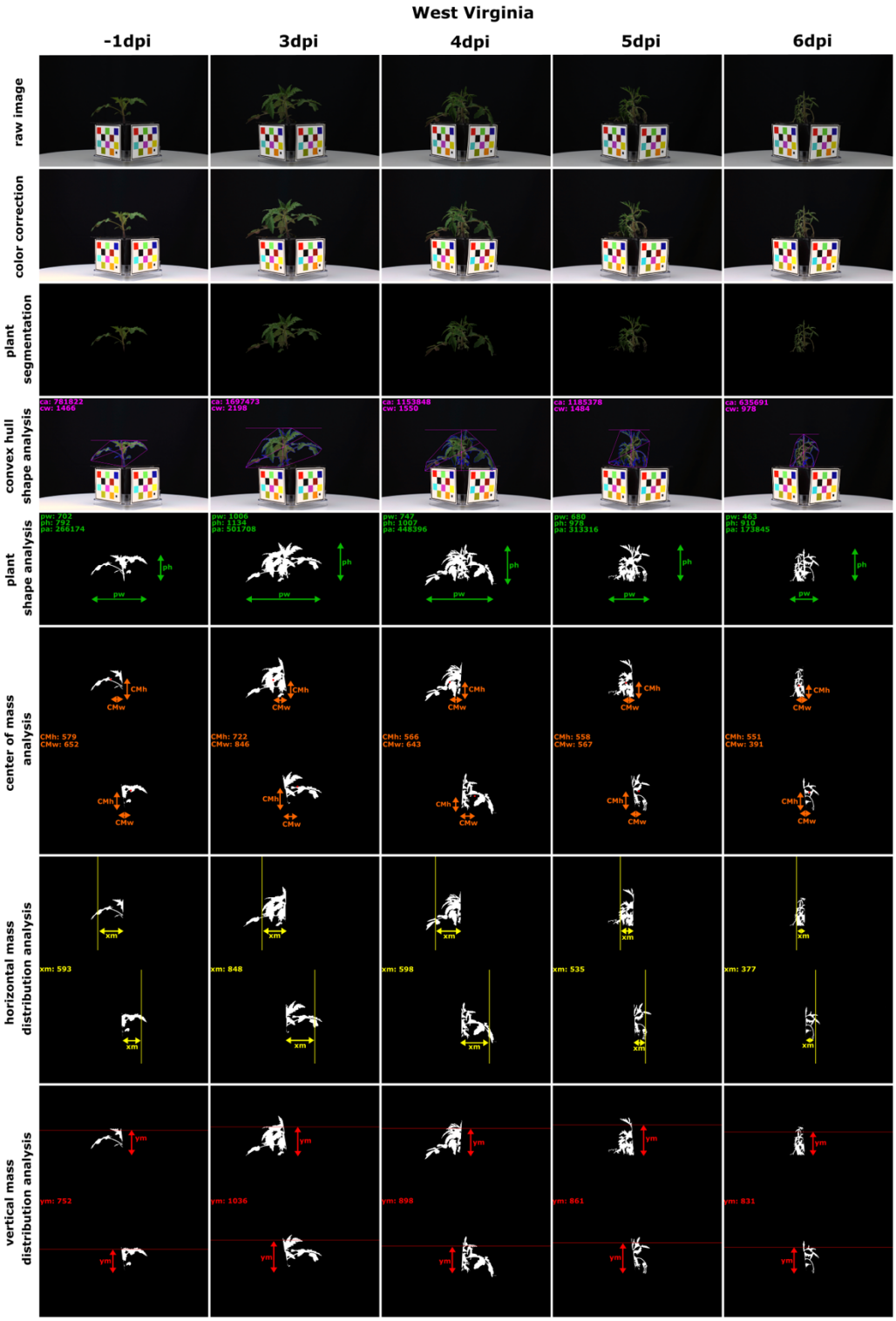
West Virginia
-1dpi
3dpi
4dpi
5dpi
6dpi
raw image
color correction
plant segmentation
convex hull shape analysis
ca: 781822
cw: 1466
ca: 1697473
cw: 2198
ca: 1153848
cw: 1550
ca: 1185378
cw: 1484
ca: 635691
cw: 978
plant shape analysis
pw: 702
ph: 797
pa: 266174
pw: 1006
ph: 1134
pa: 501708
pw: 747
ph: 1007
pa: 448396
pw: 680
ph: 978
pa: 313316
pw: 463
ph: 910
pa: 173845
center of mass analysis
CMh: 579
CMw: 652
CMh: 722
CMw: 846
CMh: 566
CMw: 643
CMh: 558
CMw: 567
CMh: 551
CMw: 391
horizontal mass distribution analysis
xm: 593
xm: 848
xm: 598
xm: 535
xm: 377
vertical mass distribution analysis
ym: 752
ym: 1036
ym: 898
ym: 861
ym: 831

Supplementary Figure 5: Boxplots showing the normalized values for image-based traits at -1, 3, 4, 5, 6 dpi for resistant Hawaii 7996, susceptible West Virginia 700, and 166 individuals of the RIL population.

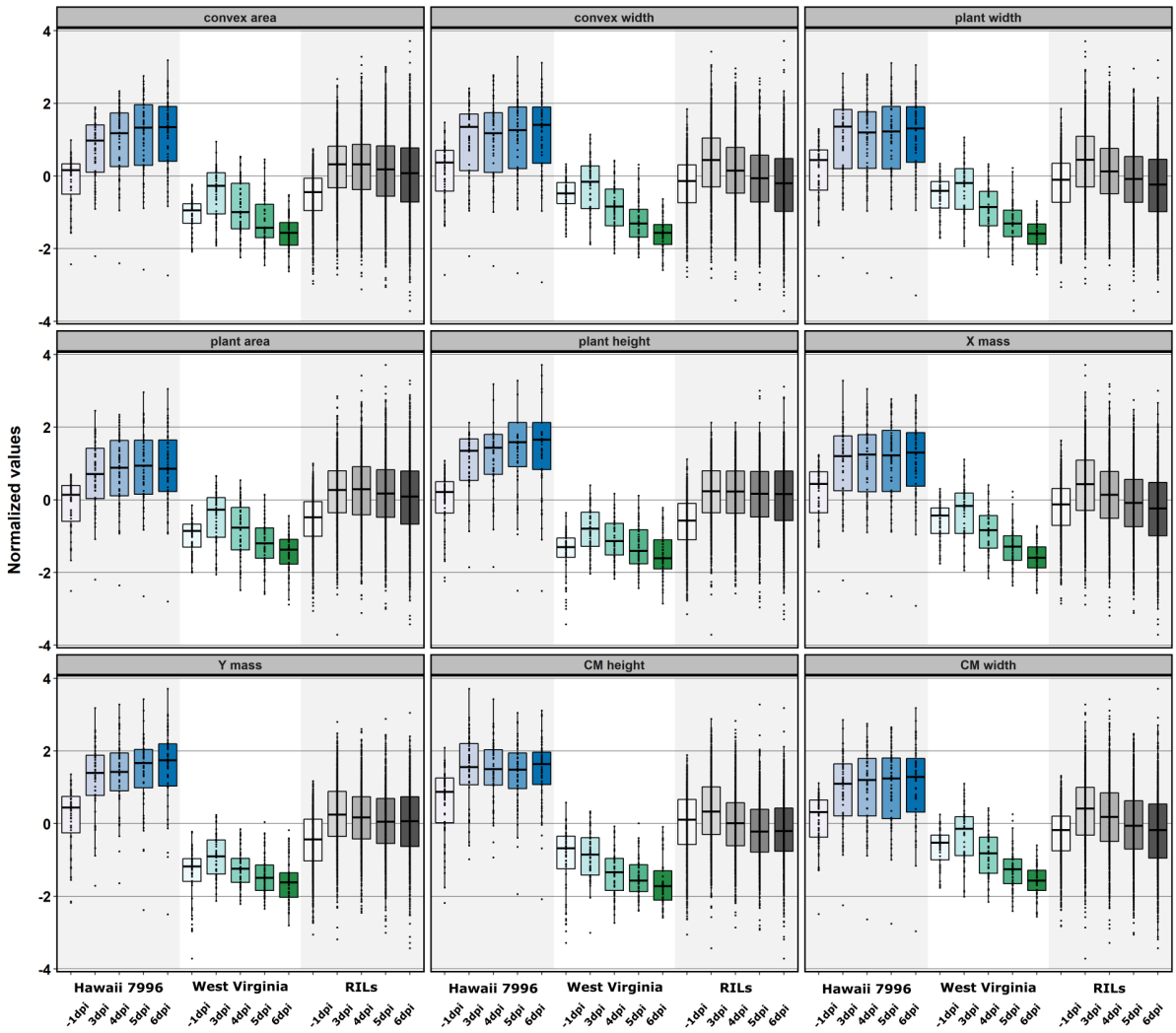

Supplementary Figure 6: Histogram showing the image-based descriptors which contribute the most to wilting

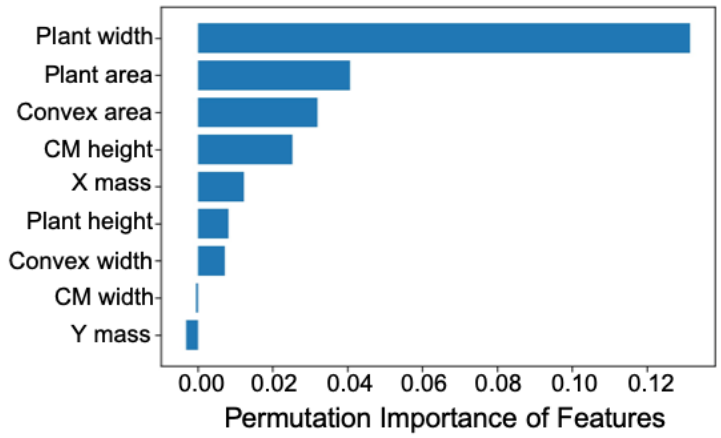

733 Supplementary Figure 7: GBS Read Distribution by Sample (includes parental references).

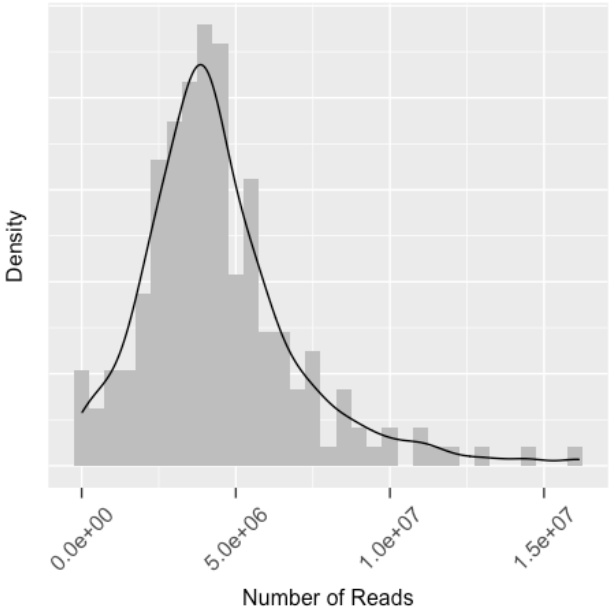

734

735

736

737

738

739

740

741

742

743

744

745

746

747

748 Supplementary Figure 8: a) RIL and parental coverage and SNP density from GBS analysis; b)

749 Percent heterozygosity and SNP density

750

751

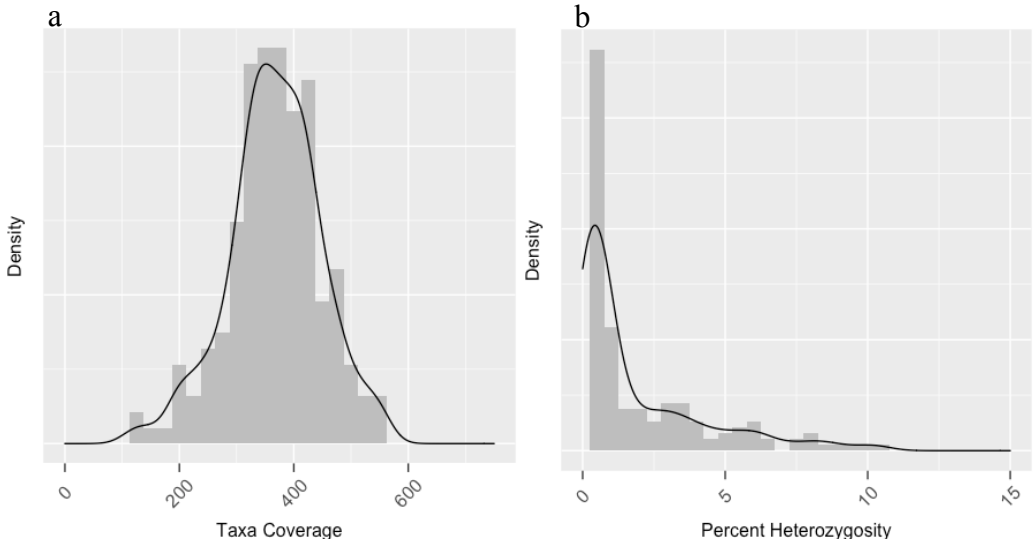

752

753

754

755

756

757

758

759

760

761

762

763

764

765

766 **Supplementary Tables**

767 Supplementary Table 1: Marker density per cM for each chromosome.

Chromosome	Number of marker	Chromosome Length (cM)	Average interval length (cM)	Standard deviation	Standard error
1	36	153.42	4.38	4.15	0.70
2	19	117.42	6.52	3.92	0.92
3	28	87.77	3.25	3.56	0.68
4	44	133.43	3.10	4.25	0.65
5	18	116.49	6.85	5.33	1.29
6	61	116.92	1.80	1.99	0.26
7	21	95.63	4.78	3.94	0.88
8	14	97.27	7.48	4.44	1.23
9	27	143.5	5.52	5.77	1.13
10	18	80.01	4.71	4.80	1.16
11	25	61.22	2.55	3.88	0.79
12	43	120.42	2.87	3.01	0.46

768

769

770

771

772 Supplementary Table 2: Overview of the 9 genomic regions identified with a LOD score superior

773 at 3 on chromosome 10 after inoculation with *R. solanacearum* at 6 dpi. According to the ICI

774 Mapping analysis using 1000 permutations, a threshold value of 3.48 represents the minimum

775 LOD to identify a significant QTL. Genomic regions with a lower LOD value did not reach our

776 threshold for significance after permutation.

Chromosome	Position	LeftMarker	RightMarker	TraitName	LOD	PVE	Add
10	51	solcap_snp_sl_33168	SL3.0ch10-63377492	Wilting Score 2019	3.0067	13.3810	0.2077
10	52	solcap_snp_sl_33168	SL3.0ch10-63377492	Wilting Score 2019	3.0927	10.5192	0.1842
10	53	solcap_snp_sl_33168	SL3.0ch10-63377492	Wilting Score 2019	3.0832	8.0396	0.1611
10	52	solcap_snp_sl_33168	SL3.0ch10-63377492	convex width	3.1634	9.0040	-0.1835
10	53	solcap_snp_sl_33168	SL3.0ch10-63377492	convex width	3.4883	7.8538	-0.1714
10	51	solcap_snp_sl_33168	SL3.0ch10-63377492	plant width	3.0398	11.1872	-0.2039
10	52	solcap_snp_sl_33168	SL3.0ch10-63377492	plant width	3.5411	10.2424	-0.1951
10	53	solcap_snp_sl_33168	SL3.0ch10-63377492	plant width	3.8661	8.8147	-0.1811
10	53	solcap_snp_sl_33168	SL3.0ch10-63377492	X mass	3.0584	7.0293	-0.1629

777

778

779 Supplementary Table 3: Overview of QTLs identified across the genome at -1, 3, 4, 5, 6 dpi with
780 *R. solanacearum*. LOD: maximum value of the Logarithm of the odd. PVE: Percentage of
781 phenotypic variance explained. Add: Additive effect, the positive and negative values indicated
782 that the alleles are introgressed from the resistant parent (Hawaii 7996) and susceptible parents
783 (WestVirginia). LeftCI and RightCI are the confidence interval calculated by a one-LOD
784 decrease from the estimated QTL position.
785

Timepoint	Chromosome	Position	LeftMarker	RightMarker	TraitName	LOD	PVE	Add	LeftCI	RightCI
-1	2	117	solcap_snp_sl_8510	solcap_snp_sl_15574	plant width	3.3851	6.4842	0.1290	114.5	117.0
-1	2	117	solcap_snp_sl_8510	solcap_snp_sl_15574	X mass	4.1424	6.8279	0.1390	114.5	117.0
-1	3	58	SL3.0ch03-61078160	solcap_snp_sl_10372	plant width	3.2538	9.4831	0.1555	56.5	64.5
-1	3	58	SL3.0ch03-61078160	solcap_snp_sl_10372	X mass	3.8291	9.4218	0.1628	56.5	64.5
-1	3	59	SL3.0ch03-61078160	solcap_snp_sl_10372	CM height	3.7940	3.6957	0.1603	56.5	63.5
-1	3	30	solcap_snp_sl_9689	solcap_snp_sl_9681	plant area	3.6327	8.0934	0.1522	24.5	34.5
-1	4	128	SL3.0ch04-1213025	solcap_snp_sl_63869	CM height	3.8063	12.0286	-0.2891	127.5	130.5
-1	6	10	SL3.0ch06-13533085	SL3.0ch06-3310762	convex area	4.7410	11.2755	0.1621	8.5	11.5
-1	6	10	SL3.0ch06-13533085	SL3.0ch06-3310762	plant width	3.5865	6.9265	0.1336	8.5	11.5
-1	6	10	SL3.0ch06-13533085	SL3.0ch06-3310762	plant area	3.5117	7.3344	0.1457	8.5	11.5
-1	6	10	SL3.0ch06-13533085	SL3.0ch06-3310762	X mass	4.8686	8.0160	0.1510	8.5	11.5
-1	6	10	SL3.0ch06-13533085	SL3.0ch06-3310762	Y mass	4.9020	9.3612	0.1757	8.5	11.5
-1	8	80	solcap_snp_sl_21461	SL3.0ch08-63373341	X mass	3.2439	5.3622	0.1230	74.5	83.5
-1	9	67	SL3.0ch09-39293163	SL3.0ch09-63338944	convex area	3.1976	7.5230	-0.1323	60.5	69.5
-1	9	36	solcap_snp_sl_26683	SL3.0ch09-4516570	CM height	4.8307	6.1460	0.2081	32.5	40.5
-1	10	71	solcap_snp_sl_8835	Le013158s_161	Y mass	3.2077	5.9734	0.1404	68.5	73.5
3	3	25	solcap_snp_sl_14355	solcap_snp_sl_9689	CM height	7.2477	18.2665	0.2584	21.5	30.5
3	3	27	solcap_snp_sl_14355	solcap_snp_sl_9689	CM width	3.5022	8.8528	0.1536	22.5	32.5
3	3	26	solcap_snp_sl_14355	solcap_snp_sl_9689	plant width	5.5180	13.9255	0.2191	21.5	27.5
3	3	26	solcap_snp_sl_14355	solcap_snp_sl_9689	X mass	4.5407	11.7470	0.1991	22.5	32.5
3	3	39	solcap_snp_sl_21215	solcap_snp_sl_9663	convex width	5.6025	13.8198	0.2120	37.5	42.5
3	3	28	solcap_snp_sl_9689	solcap_snp_sl_9681	plant height	4.5094	10.3345	0.1974	25.5	31.5
3	3	28	solcap_snp_sl_9689	solcap_snp_sl_9681	Y mass	5.7227	15.0239	0.2325	23.5	31.5
4	3	39	solcap_snp_sl_21215	solcap_snp_sl_9663	convex width	3.9750	10.2036	0.1829	37.5	43.5
4	3	39	solcap_snp_sl_21215	solcap_snp_sl_9663	CM width	4.5294	8.4260	0.1853	37.5	43.5
4	3	39	solcap_snp_sl_21215	solcap_snp_sl_9663	plant width	3.8768	9.9017	0.1838	37.5	43.5
4	3	39	solcap_snp_sl_21215	solcap_snp_sl_9663	X mass	3.8156	9.7282	0.1837	37.5	43.5
4	3	28	solcap_snp_sl_9689	solcap_snp_sl_9681	convex area	3.1310	7.7809	0.1508	22.5	32.5
4	3	30	solcap_snp_sl_9689	solcap_snp_sl_9681	plant area	3.8685	9.9594	0.1672	23.5	33.5
5	3	22	solcap_snp_sl_14355	solcap_snp_sl_9689	CM height	3.6770	9.3886	0.1414	21.5	27.5
5	3	22	solcap_snp_sl_14355	solcap_snp_sl_9689	plant width	3.4953	9.3017	0.1806	21.5	27.5
5	3	25	solcap_snp_sl_14355	solcap_snp_sl_9689	plant height	3.6851	8.5381	0.1738	21.5	31.5
5	3	25	solcap_snp_sl_14355	solcap_snp_sl_9689	Y mass	3.4687	9.9830	0.1673	21.5	31.5
5	3	39	solcap_snp_sl_21215	solcap_snp_sl_9663	convex width	3.7859	9.8306	0.1891	37.5	43.5
5	3	39	solcap_snp_sl_21215	solcap_snp_sl_9663	CM width	4.0630	7.4955	0.1924	35.5	39.5
5	5	107	SL3.0ch05-65105663	SL3.0ch05-66111590	plant height	3.4091	8.9327	0.1778	104.5	114.5
5	12	56	SL3.0ch12-62154155	solcap_snp_sl_19345	CM height	3.2828	8.2102	0.1360	54.5	59.5
6	2	72	SL3.0ch02-45885016	SL3.0ch02-44375028	X mass	3.4765	9.4924	-0.2178	69.5	73.5
6	2	72	SL3.0ch02-45885016	SL3.0ch02-44375028	CM width	3.2455	8.4550	-0.2189	69.5	73.5
6	2	45	solcap_snp_sl_18519	SL3.0ch02-49265134	plant width	3.4108	6.4576	-0.1669	42.5	47.5
6	3	22	solcap_snp_sl_14355	solcap_snp_sl_9689	convex width	5.3238	10.2506	0.2103	21.5	26.5
6	3	22	solcap_snp_sl_14355	solcap_snp_sl_9689	plant width	4.7309	9.1511	0.1976	21.5	25.5
6	3	25	solcap_snp_sl_14355	solcap_snp_sl_9689	plant height	4.5107	7.6902	0.1896	21.5	31.5
6	3	23	solcap_snp_sl_14355	solcap_snp_sl_9689	CM width	3.6627	6.2716	0.1887	21.5	27.5
6	3	22	solcap_snp_sl_14355	solcap_snp_sl_9689	X mass	3.4765	5.8012	0.1705	21.5	26.5
6	3	25	solcap_snp_sl_14355	solcap_snp_sl_9689	Y mass	3.3918	9.3283	0.1708	21.5	31.5
6	3	38	solcap_snp_sl_21215	solcap_snp_sl_9663	Wilting Score 2016	3.5258	7.3736	-0.1726	35.5	39.5
6	3	38	solcap_snp_sl_21215	solcap_snp_sl_9663	convex area	3.4328	9.0796	0.1953	34.5	39.5
6	3	38	solcap_snp_sl_21215	solcap_snp_sl_9663	plant area	3.3019	8.6697	0.1902	34.5	39.5
6	4	4	SL3.0ch04-60431371	solcap_snp_sl_11543	convex width	3.1855	6.0199	0.1627	1.5	10.5
6	5	100	solcap_snp_sl_22649	SL3.0ch05-65105663	plant height	3.6115	9.4852	0.2103	95.5	103.5
6	6	79	solcap_snp_sl_14458	SL3.0ch06-39435402	Wilting Score 2016	4.0770	8.7626	-0.1871	76.5	81.5
6	6	81	solcap_snp_sl_14458	SL3.0ch06-39435402	Wilting Score 2019	3.2673	11.0473	-0.1621	78.5	81.5
6	10	53	solcap_snp_sl_33168	SL3.0ch10-63377492	plant width	3.8661	7.6897	-0.1811	50.5	54.5
6	10	53	solcap_snp_sl_33168	SL3.0ch10-63377492	convex width	3.4883	6.8155	-0.1714	50.5	54.5
6	12	37	solcap_snp_sl_1525	solcap_snp_sl_1572	CM height	4.1755	10.7222	0.1837	33.5	40.5
6	12	42	solcap_snp_sl_58807	solcap_snp_sl_9707	Y mass	3.3249	8.5939	0.1651	40.5	43.5

787